COMPARATIVE STUDY OF TRANSFER MATRIX FORMALISM VS SINGLE-MODE MODEL FOR SEMICONDUCTOR MICROCAVITIES

by

Mario Carcamo

A Thesis Submitted to the Faculty of the

JAMES C. WYANT COLLEGE OF OPTICAL SCIENCES

In Partial Fulfillment of the Requirements

For the Degree of

MASTER OF SCIENCE

In the Graduate College

THE UNIVERSITY OF ARIZONA

2020

THE UNIVERSITY OF ARIZONA
GRADUATE COLLEGE

As members of the Master's Committee, we certify that we have read the thesis prepared by Mario Carcamo titled *Comparative Study of Transfer Matrix Formalism vs Single-Mode Model for Semiconductor Microcavities* and recommend that it be accepted as fulfilling the dissertation requirement for the Master's Degree.

DocuSigned by:
Rolf Binder
B4AB8B1F48204E7...

Rolf Binder Date: 1/15/2020

DocuSigned by:
Ewan Wright
1AAA653284D44D6...

Ewan Wright Date: 1/15/2020

DocuSigned by:
Khanh Kieu
9F8BB3B0A620436...

Khanh Kieu Date: 1/15/2020

Final approval and acceptance of this thesis is contingent upon the candidate's submission of the final copies of the thesis to the Graduate College.

I hereby certify that I have read this thesis prepared under my direction and recommend that it be accepted as fulfilling the Master's requirement.

DocuSigned by:
Rolf Binder
B4AB8B1F48204E7...

Rolf Binder Date: 1/15/2020
Master's Thesis Committee Chair
Department of Optical Sciences

CONTENTS

LIST OF FIGURES. 4

ABSTRACT. 7

1 INTRODUCTION. 8

2 TRANSFER MATRIX METHOD AND PROBLEM STATEMENT 9
2.1 Transfer Matrices 9
2.1.1 Propagation Matrix 9
2.1.2 Interface Matrix 10
2.1.3 QW Matrix 11
2.2 Extracting Information From the Model 11
2.2.1 Reflectance and Transmittance 11
2.2.2 E-Field in Frequency Domain 12
2.2.3 E-Field in Time Domain 13
2.3 Working Model for the Microcavity 14
2.3.1 Field in the Various Regions 14
2.3.2 Field at the Quantum Well 16
3 THE MICROCAVITY 18
3.1 The Cavity without QW 18
3.1.1 Reflectance and E-field 19
3.2 Cavity with the Quantum Well 21
3.2.1 Evaluating the Quantum Well Matrix 21
3.2.2 Reflectance and E-Field Amplitude in Spatial Domain 21
3.3 Propagation of a Gaussian Pulse 24
3.3.1 Pulse Shape 24
3.3.2 Short Pulse and Time of Flight 24
3.3.3 Narrow Bandwidth pulse 24
4 TESTING AND DEBUGGING 27
4.1 Dielectric Slab 27
4.1.1 Setting Up The Matrices 27
4.1.2 Computing Reflectance and Mode Spacing 28
4.1.3 Comparing Results 28
4.2 DBR Mirrors 30
4.3 Single Layer Test 32
4.4 Exponential Decay of Response Function 34
5 RESULTS. 35
5.1 Preparing the Phenomenological Approach for Comparison 35
5.1.1 Positive Frequencies and Envelope 36
5.1.2 Cavity Coefficients 37
5.2 Reevaluating the Gaussian Pulse 37
APPENDIX 41

REFERENCES 48

List of Figures

Figure 2.1 Working diagram of the cavity. This generalizes each region with labels to do some preliminary investigations. A working theoretical model is created out of these labels. The multilayer DBRs are symbolically represented by a single interface. It should be noted that there is no left propagating light on the right side of the cavity as we are limiting ourselves to only having incoming light in a single direction. The subscripts of the E-Field denote which region they represent. 14

Figure 3.1 Diagram of cavity without the quantum well. This figure adds more detail than the previous figure of the cavity being modeled. Although the quantum well is not included in this setup, the details of the DBRs are demonstrated here. A layer is actually a pair of two layers which together make a couple. There are 17 of those (or 35 actual slabs/layers if you count the layer in between). The matrix below the first DBR demonstrates the nature of the matrices that build the total matrix that represents the DBR. The second DBR has a similar matrix to represent its structure. The dots in between the layers of each DBR signify that there are more repetitive layers not shown explicitly. 18

Figure 3.2 Here we have a reflectance profile of a pair of DBRs. The resonance coincides with the thickness of the alternating layers but also the separation of the DBRs. The x-axis is corresponding to frequencies of light with that particular energy. The broadness can be attributed to the seperation of the two DBRs. It should be noted that at resonance, the cavity resorts to the natural reflectance of 0.25 which corresponds from the reflection between a medium with index $n_1 = 1.0$ and $n_2 = 3.0$. This is the profile of the cavity before the quantum well is inserted. 19

Figure 3.3 We demonstrate other behaviors of our cavity in these figures. The left figure shows that at larger separations, keeping the separation a multiple of the resonant wavelength, causes the dip to be much sharper as it is harder for off resonant light to survive in this cavity. The right shows what happens when we set an arbitrary seperation. The resonance shifts accordingly to represent the new mode its able to support 20

Figure 3.4 These figures show how the amplitude of the electric field varies through the cavity in the case that the cavity is seperated by two $\lambda/4$ layers. This is therefore the setup of the cavity being used throughout the rest of the investigation. For now the quantum well is excluded though. The field amplitude was divided by the amplitude of the incoming light and squared so as to show a relative field strength and to be able to compare both cases. The plots have a data point for every interface in the cavity. At one layer you have some stable level of light and then at the interface for the next layer a standing wave node 20

Figure 3.5 Diagram of the cavity with quantum well. At this point, we finally introduce the quantum well in the setup. It should be noted that the actual quantum well is assumed to have zero thickness which makes this diagram a bit misleading. The DBRs are of the same structure presented previously with alternating indices and 17 coupled layers. 21

Figure 3.6 Reflectance of the total cavity. This is a comparable figure to 3.2 in the sense that it demonstrates exactly what happens after the quantum well is introduced. The resonance splits into two resonances with one being the lower polariton (LP) and the other the upper polariton (UP) resonances. It should be noted that there is some structure to this resonance beyond this range of energy levels but these are the ones of interest. Later on, to perform various calculations, a much larger domain must be used. 22

Figure 3.7 The propagation of the E-field amplitude is demonstrated in these figures. The behavior is very similar to the case without the quantum well where resonant light gets amplified at the center of the cavity. Again, the plots have a data point for every interface in the cavity. At one layer you have some stable level of light and then at the interface for the next layer a standing wave node. 22

Figure 3.8 Off resonant light was used as a means to make sure the simulated model was working as it should. This behavior is what was expected and so this gives a certain amount of assurance to the results. Much like the off resonant no quantum well case in the previous section, the amplitude of the field quickly dies out as the off resonant field is highly reflective and so the resonator will not sustain this frequency of light. 23
Figure 3.9 This figure shows the first attempts at finally doing something meaningful with our simulations. The behaviors of injecting a gaussian pulse into the cavity were deduced by our models and shown here. A broad gaussian was used so that the corresponding pulse in the time domain would be sharper and easier to resolve its peaks. This is also to reduce the overlap as the pulse needed to be shorter than the actual cavity. The left graph shows the frequency spectrum of the incoming light and the right shows the incoming pulse followed by the pulse once it reaches the quantum well. The peaks were resolved and the time difference calculated to make sure the time difference agrees with the time of flight calculated. These fields were not squared however, like previous amplitude models, so as to show the negative oscillations in the figures. 25
Figure 3.10 As opposed to the previous gaussian use, this one is much more narrow in the frequency domain which leads to a much broader pusle in the time domain. The extreme amount of overlap in the time domain is due to that fact. The field in the time domain is plotted as a relative strength to the incoming light. These fields were not squared, like previous amplitude models, however so as to show the negative oscillations in the figures. Ultimately, we are interested in the e-field at the quantum well so we want to see these oscillations as well. . . . 25
Figure 4.1 Diagram of the dielectric slab. The indices are labeled so as to coincide with the derivations in the section. 27
Figure 4.2 Gamma Term superimposed on the numerical results so as to demonstrate that our numerical results are mode spaced as they should be. The actual amplitudes are not significant as we are only trying to demonstrate mode spacing. It would also prove difficult to resolve if the amplitudes were the same as they would completely overlap. 28
Figure 4.3 The results obtained numerically are compared to the literature. It should be obvious which bands correspond to each other between the two graphs but a legend was provided to avoid confusion. Some deformation may be witnessed due to scaling and such but the results were also compared numerically just to confirm that they are in fact the same. 29
Figure 4.4 Diagram of the DBR. The dots are there to represent any arbitrary number of layers. This diagram very much coincides to the diagram used in the earlier sections to demonstrate the cavity so as to keep the same conventions. In this case however, we manipulate the number of layers. 30
Figure 4.5 This shows the reflectances obtained through numerical simulations and from the literature. The results are artificially shifted by 0.1 to show that they have the same shape. The x-axis is the amount of coupled layers not to be confused with actual layers as each coupled layers counts for 2 different index layers. 31
Figure 4.6 Diagram of the single layer setup. The figure demonstrates the convention used for the derivations to follow. Again, note that the quantum well is actually assumed to have no thickness despite what is being demonstrated in this figure. 32
Figure 4.7 Reflectance of single layer cavity as a function of energy corresponding to different frequencies of light. 33
Figure 4.8 The HWHM maximum of the empty cavity was deduced numerically as shown in Figure (a). Later it was fitted to Figure (b) to show that the response function of the empty cavity has an exponential decay corresponding to that metric. 34

Figure 5.1 Here we have both the real and imaginary parts of $a(\omega)$ in frequency space. The nature of the integrals can be determined by basic observations of the symmetries shown in these graphs. Of interest is the oscillations found in between resonances. These are a product of using the Transfer Matrix Method over the single-mode equations. These deviations show how the two methods are in disagreement with each other and can be a source of error when choosing the domain of which to integrate over. It is shown later that this error is negligible. 36
Figure 5.2 In Figure(a) we have both the real and imaginary parts of $b(\omega)$ in frequency space. Figure (b) shows a combination of $a(\omega)$ and $b(\omega)$ to form all the coefficients used in the integrand. 37
Figure 5.3 This is a plot of $C(t-t')$, the response function used to emulate the entire cavity. . . 38
Figure 5.4 This figure shows the results of a gaussian pulse incident on the cavity. Figure (a) shows the response without a quantum well using a gaussian with $\hbar\omega_0 = 1.599eV$ and Figure (b) shows the response with the quantum well using a gaussian with $\hbar\omega_0 = 1.593eV$. These gaussians used the same $\hbar\sigma_\omega$ of $0.9meV$ and therefore each incident pulse had the same pulse duration. A $\hbar\Delta\omega$ of 0.5 eV was used for the domain which corresponds to a $\hbar\omega_{min} = 1.594eV$ and $\hbar\omega_{max} = 1.604eV$ for the second graph and $\hbar\omega_{min} = 1.589eV$ and $\hbar\omega_{max} = 1.598eV$ for the second graph 39
Figure 5.5 $A(t)$ obtained using different domains. The blue curve used an $a(\omega)$ that extended to 1.5 eV outside resonance on both of its sides (corresponding to a domain width of 3 eV) while the red curve extend only to 0.5 eV. The larger domain saw more of the outer oscillating structures of $a(\omega)$ causing the discrepancy. The graph on the right had better resolution which allowed for resolving the oscillations due to using a wider domain. 40
Figure 5.6 The results demonstrate not only the discrepancies between the integrals but also the senstivity of the model to using a larger domain. It is with this resolution that you can see the negligible difference between the different integrals. The red dashed curve is the bounded integral and the blue is the full integral. Like Figure 5.4b a $\hbar\omega_0 = 1.593eV$ was usd but using different frequency domain widths. 40

Abstract

An optical semiconductor micrcavity consisting of two distributed bragg reflectors (DBRs) and a quantum well between, can be modeled using a transfer matrix approach, which solves the propagation through the DBR mirrors and the cavity segment in between the mirrors. Such an approach is easy to use if the interband polarization of the quantum well P_{QW} is a given function of time or frequency, which includes the case of linear optical response, where P_{QW} is given in terms of the linear susceptibility and the electric field at the position of the quantum well, E_{QW}. In many cases of practical interest, the quantum well response is a nonlinear function of E_{QW}, in which case the transfer matrix approach becomes impractical. In such cases, a time differential equation for P_{QW}, which is of the form

$$i\hbar \frac{dP_{QW}(t)}{dt} = F[P_{QW}(t), E_{QW}(t)]$$

where F is a nonlinear function of P_{QW}, is solved via time-stepping from earlier to later times. To obtain the electric field E_{QW} needed as input to the P_{QW} solution, a commonly used phenomenological approach utilizes the single-mode equation

$$i\hbar \frac{dE_{QW}(t)}{dt} = h\omega_c E_{QW}(t) - \Omega P_{QW}(t) + S(t)$$

with the source term $S(t)$ being defined by

$$S(t) = \hbar t_c E^+_{inp}(t)$$

and corresponding constants that are defined in section 5 of this thesis. However, apart from containing phenomenological parameters, the simple source term entering the single-mode equation does not account for propagation, retardation, and pulse filtering effects of the incident light field traversing the DBR mirror. In this thesis, an alternate approach is presented along with evidence of its validity using a bounded convolution integral instead. The integral is used to determine the electric field as a function of time and therefore can be used to determine the time derivative of the polarization. The integral being

$$E_{QW}(t) = \int_{-\infty}^{t} [A(t-t')E^+_{inp}(t') + B(t-t')P_{QW}(t')]dt'.$$

We show in the final sections that it is adequate to use this bounded integral to resolve pulses in the time domain. Evidence of that is done using a gaussian pulse and linear response. This method could then be used in conjunction with a time stepping algorithm to resolve nonlinear responses.

1 Introduction

The optical semiconductor microcavity is a physical system that has been modeled and examined thoroughly throughout history. It has characteristics that allows one to explore interesting physics. Various configurations of an optical cavity exist but typically it consists of optical components that form a resonator that support standing wave modes. One of the more common uses for this type of system is to excite a gain medium to produce a laser. However, for this thesis we limit ourselves to a configuration. The cavity being explored will essentially be two distributed bragg reflectors or DBRs that encapsulate a piece of semiconductor material that acts as a quantum well.

This cavity was modeled using a transfer matrix approach. In other words, information regarding the reflected, transmitted, and incident light was assessed in order to determine the overall behavior as light propagates through this physical system. Matrices were used to mathematically represent how light transforms as it experiences the different parts in the cavity.

Previous work in using this approach was limited to determining the electric field in the quantum well. In this thesis, the transfer matrix model was extended to produce the electric field as a function of time using a bounded integral. The goal is to demonstrate that by bounding the integral we still obtain the same results. From there one could resolve the field at any point in the cavity such as the reflected field.

In this thesis we limit ourselves to a semiconductor microcavity consisting of two DBRs and GaAs as the quantum well in the center, but this model can be extended to other configurations of interests such as the ones used for TMDs in [6]. DBRs are constructed using alternating index /4 layers where is the wavelength corresponding to the resonant light to the quantum well material. These DBR's produce a cavity mode which interacts strongly with the quantum well which we model.

The thesis is laid out as follows. Chapter 2 dives into the transfer matrix approach and the basic algorithms to use it. Chapter 3 extends that model into a more general space so that any arbitrary source of light can be used. It also shows how to extract the electric field in the time domain. Chapter 4 focuses on how this approach was stress tested. Various metrics were used to reassure that the simulations was producing the right results. Chapter 5 finally tackles the overarching problem. It presents the results and the final parts of the project that led up to them. Finally, it demonstrates how the proposed convolution integral can resolve a gaussian pulse using linear response.

2 Transfer Matrix Method and Problem Statement

An overview of the Transfer Matrix Method will be presented bellow. The goal is to simulate light in a microcavity consisting of two DBR mirrors and a semiconductor quantum well at the center. With this method we will be able to deduce the state of the electric field at every point inside and outside the cavity as a function of frequency. We will evaluate the model for the case of normal incident light to simplify the calculations. A slightly more advanced approach to modeling the light will be shown in later sections. More about this approach can be found in Ch.3 of [7] or in [12].

2.1 Transfer Matrices

The relation between the pumping field and resultant electric field can be generalized to this form when you only have right propagating light at the input

$$\begin{pmatrix} E_t \\ 0 \end{pmatrix} = M_{Total}^{TE/TM} \begin{pmatrix} E_i \\ E_r \end{pmatrix}, \tag{2.1}$$

where $M_{Total}^{TE/TM}$ is a matrix that models the transformation that is undergone in the cavity. Reflectance and Transmittance can be derived using the components of this matrix. The pumping field which is incident on the cavity can either be TE or TM. For TE light we have the following generalized form

$$E(x,y,z,\omega_p) = E_y^+(z,\omega_p)e^{ixk_x}e^{izk_z}\hat{y} + E_y^-(z,\omega_p)e^{ixk_x}e^{-izk_z}\hat{y}\ , \tag{2.2}$$

where E_y^+ corresponds to the transmitted direction and E_y^- correpsonds to the reflected direction. For TM light the auxiliary field will now be in the transverse direction and we will have

$$H(x,y,z,\omega_p) = H_y^+(z,\omega_p)e^{ixk_x}e^{izk_z}\hat{y} + H_y^-(z,\omega_p)e^{ixk_x}e^{-izk_z}\hat{y}\ , \tag{2.3}$$

as our generalized equation with the same notation with regards to direction. Since we are limiting ourselves to normal incident light, we must set k_x to zero (the k vector will lack an x component)

$$\boxed{\begin{aligned} E(x,y,z,\omega_p) &= E_y^+(z,\omega_p)e^{izk_z}\hat{y} + E_y^-(z,\omega_p)e^{-izk_z}\hat{y}, \\ H(x,y,z,\omega_p) &= H_y^+(z,\omega_p)e^{izk_z}\hat{y} + H_y^-(z,\omega_p)e^{-izk_z}\hat{y} \end{aligned}} \tag{2.4}$$

These are the forms of the generalized pumping fields.

2.1.1 Propagation Matrix

Inside of a dielectric material, the light will obtain a phase factor $\vec{z}\cdot\vec{k} = \omega_p n\cos\theta\Delta z/c_0$, where $\vec{z} = \Delta z\hat{z}$ is the displacement the light travels, n the refractive index, and θ is the angle of propagation with respect to the $\hat{z}$ axis. We can define the transfer matrix as

$$M_P(n,\theta,\Delta z) = \begin{pmatrix} e^{i\frac{\omega_p n\cos\theta}{c_0}\Delta z} & 0 \\ 0 & e^{-i\frac{\omega_p n\cos\theta}{c_0}\Delta z} \end{pmatrix}, \tag{2.5}$$

but since we are limiting ourselves to normal incidence the matrix simplifies to

$$\boxed{M_P(n,\Delta z) = \begin{pmatrix} e^{i\frac{\omega_p n}{c_0}\Delta z} & 0 \\ 0 & e^{-i\frac{\omega_p n}{c_0}\Delta z} \end{pmatrix}} \tag{2.6}$$

which when applied to the field will give the resultant displaced field through this relation

$$\begin{pmatrix} E_y^+(z+\Delta z,\omega_p) \\ E_y^-(z+\Delta z,\omega_p) \end{pmatrix} = M_P(n,\theta,\Delta z)\begin{pmatrix} E_y^+(z,\omega_p) \\ E_y^-(z,\omega_p) \end{pmatrix}, \tag{2.7}$$

This gives you the resultant field after it propagates a distance Δz. Note that this matrix is independent of the mode the light is in.

2.1.2 Interface Matrix

In the cavity, the light will also interact with dielectric media in the form of the DBR mirrors which can be modeled using snell's law,

$$n_1 \sin\theta_1 = n_2 \sin\theta_2 \tag{2.8}$$

the boundary conditions imposed by maxwell's equations,

$$\begin{aligned} E_{x1} &= E_{x2} \\ H_{x1} &= H_{x2} \end{aligned} \tag{2.9}$$

and the relation between the two fields,

$$H_i = (n_i/\mu c_0)\hat{k} \times \hat{E}_i \tag{2.10}$$

you can construct a matrix that produces the resultant field when the electric field meets a dielectric boundary. The matrix however is dependent on the mode of light. For TE light we use the following matrix derived from the conditions imposed by the boundary conditions

$$M_I^{TE}(n_1, n_2, \theta_1, \theta_2) = \frac{1}{2n_2 \cos\theta_2} \begin{pmatrix} n_2\cos\theta_2 + n_1\cos\theta_1 & n_2\cos\theta_2 - n_1\cos\theta_1 \\ n_2\cos\theta_2 - n_1\cos\theta_1 & n_2\cos\theta_2 + n_1\cos\theta_1 \end{pmatrix}, \tag{2.11}$$

evaluated at normal incidence becomes

$$\boxed{M_I^{TE}(n_1, n_2) = \frac{1}{2n_2} \begin{pmatrix} n_2 + n_1 & n_2 - n_1 \\ n_2 - n_1 & n_2 + n_1 \end{pmatrix}} \tag{2.12}$$

where n_1 pertains to the initial medium and n_2 pertains to the medium the light is incident on. The matrix for TM light takes a different form. The matrix is as follows

$$M_I^{TM}(n_1, n_2, \theta_1, \theta_2) = \frac{1}{2n_2 \cos\theta_2} \begin{pmatrix} n_1\cos\theta_2 + n_2\cos\theta_1 & n_1\cos\theta_2 - n_2\cos\theta_1 \\ n_1\cos\theta_2 - n_2\cos\theta_1 & n_1\cos\theta_2 + n_2\cos\theta_1 \end{pmatrix}, \tag{2.13}$$

evaluated at normal incidence becomes

$$\boxed{M_I^{TM}(n_1, n_2) = \frac{1}{2n_2} \begin{pmatrix} n_2 + n_1 & n_1 - n_2 \\ n_1 - n_2 & n_2 + n_1 \end{pmatrix}} \tag{2.14}$$

At normal incidence the two matrices take similar form for both modes of light. The input and output field are therefore related in this way

$$\begin{pmatrix} E_{y2}^{+}(z, \omega_p) \\ E_{y2}^{-}(z, \omega_p) \end{pmatrix} = M_I(n_1, n_2) \begin{pmatrix} E_{y1}^{+}(z, \omega_p) \\ E_{y1}^{-}(z, \omega_p) \end{pmatrix}. \tag{2.15}$$

2.1.3 QW Matrix

A matrix based off the lorentzian oscillator model is used to determine what occurs at a Quantum Well. The susceptibility, which is derived from this model, takes this form

$$\boxed{\chi(\omega) = -|\vec{d}|^2 \frac{|\Omega_{ls}(r=0)|^2}{\hbar\omega - \varepsilon_x + i\gamma_x}} \tag{2.16}$$

where $|\vec{d}| = e < c|\vec{r}|v >$ is the expectation value of the electric dipole moment with $\vec{r}$ being the position vector between the valence and conduction band, $\Omega_{ls}(r=0) = \frac{2\sqrt{2}}{a_0\sqrt{\pi}}$ is the two-dimensional real space 1s exciton wavefunction at zero electron-hole separation $r = 0$, and a_0 is the 3D exciton bhor radius. A complete derivation can be found in [10]. The total matrix is dependent on the mode of light. You have the following two matrices depending on the mode of light

$$M_{QW}^{TE}(n, \omega_p, \theta) = \begin{pmatrix} 1 & 0 \\ 0 & 1 \end{pmatrix} + 2\pi i \frac{\omega_p}{c_0 n \cos\theta} \chi(\omega p) \begin{pmatrix} 1 & 1 \\ -1 & -1 \end{pmatrix}, \tag{2.17}$$

$$M_{QW}^{TM}(n, \omega_p, \theta) = \begin{pmatrix} 1 & 0 \\ 0 & 1 \end{pmatrix} + 2\pi i \frac{\omega_p \cos\theta}{c_0 n} \chi(\omega p) \begin{pmatrix} 1 & 1 \\ -1 & -1 \end{pmatrix}, \tag{2.18}$$

which of course become identical when you have normal incidence. The $\cos\theta$ term becomes 1. Similar to the previous matrix, you multiply this matrix to the vector form of the electric field to get the modified field after it passes the QW

$$\begin{pmatrix} E_{y2}^{+}(z, \omega_p) \\ E_{y2}^{-}(z, \omega_p) \end{pmatrix} = M_{QW}(n, \omega_p, \theta) \begin{pmatrix} E_{y1}^{+}(z, \omega_p) \\ E_{y1}^{-}(z, \omega_p) \end{pmatrix} \tag{2.19}$$

2.2 Extracting Information From the Model

As you propagate light through your optical configuration, the values of the column vector are the amplitudes of the field at that specific location. To determine the amplitude in the spatial domain, one simply needs to take note of the value of the vector as you multiply through the matrices. These amplitudes will be what they are exactly after propagation or after transfering to a different medium. To get the field at an arbitrary later location z, you unpack the array by multiplying it with a propagation matrix as shown previously in equation 2.15. There are however other features that can be extracted from this model which will be shown in the sections that follow.

2.2.1 Reflectance and Transmittance

The reflectance and transmittance of an optical system can be determined by properly setting up these matrices to model your optical system. Using equation 2.1 and solving the system of equations once the total matrix is determined, one can compute the reflectance and transmittance.

$$\begin{pmatrix} E_t \\ 0 \end{pmatrix} = \begin{pmatrix} M_{11}^T & M_{12}^T \\ M_{21}^T & M_{22}^T \end{pmatrix} \begin{pmatrix} E_i \\ E_r \end{pmatrix}. \tag{2.20}$$

Here we denote the total matrix using M^T and we label its different components using the subscripts. Solving for the incident, reflected, and transmitted fields you get this system of equations

$$\begin{aligned} E_t &= M_{11}^T E_i + M_{12}^T E_r \\ 0 &= M_{21}^T E_i + M_{22}^T E_r. \end{aligned} \tag{2.21}$$

This then simplifies to the following relations

$$E_r = -\frac{M_{21}^T}{M_{22}^T} E_i$$
$$E_t = (M_{11}^T - \frac{M_{21}^T}{M_{22}^T}) E_i. \tag{2.22}$$

Reflectance and transmittance are by definition

$$R = |\frac{E_r}{E_i}|^2$$
$$T = |\frac{E_t}{E_i}|^2. \tag{2.23}$$

The reflectance and transmittance then are simply

$$\boxed{\begin{aligned} R &= |-\frac{M_{21}^T}{M_{22}^T}|^2 \\ T &= |M_{11}^T - \frac{M_{21}^T}{M_{22}^T}|^2 \end{aligned}} \tag{2.24}$$

2.2.2 E-Field in Frequency Domain

The total matrix is dependent on the cavity and its optical configuration. So far, the approach is only able to handle a single frequency at a time. In order to generalize this however is fairly simple. If you are trying to model light with a specific spectrum, the way you would go about figuring out how the spectrum would change through your configuration is by running through every frequency independently, computing the reflectance and transmittance for each frequency, and then changing the amplitude of that frequency in your original spectrum. Your final spectrum will just be

$$E_t(\omega) = (M_{11}^T - \frac{M_{21}^T}{M_{22}^T})_\omega E_i(\omega), \tag{2.25}$$

in which the subscript in front of the matrix terms just denotes that the total matrix has a dependence on frequency that is discrete. Here $E_i(\omega)$ is the incident field and $E_t(\omega)$ is the transmitted field. This is limited to just determining the input and output fields. To generate the field at any arbitrary point in a particular configuration you simply need to propagate the array,

$$\begin{pmatrix} E_i(\omega) \\ -\frac{M_{21}^T(\omega)}{M_{22}^T(\omega)} E_i(\omega) \end{pmatrix}, \tag{2.26}$$

to the location in question using a subset of the original matrices you used to compute M^T. Say your total matrix has the form

$$M_{total} = M_n M_{n-1} ..... M_1, \tag{2.27}$$

where the matrices are some combination of interface, propagation, and quantum well matrices. To figure out the field at a specific location, say at an interface that is being represented by a matrix M_m at location m where $m < n$ (less than the total amount of matrices for the whole configuration) you would then multiply the matrices up to that point

$$\begin{pmatrix} E_m^+(\omega) \\ E_m^-(\omega) \end{pmatrix} = M_m M_{m-1} ..... M_1 \begin{pmatrix} E_i(\omega) \\ -\frac{M_{21}^T(\omega)}{M_{22}^T(\omega)} E_i(\omega) \end{pmatrix}. \tag{2.28}$$

Note that the array is still in terms of the total matrix hence knowledge of the total optical configuration must be known to evaluate the field at one of its arbitrary locations. Unpacking the array to the full field at an arbitrary location (labeled with subscript m) will then just be

$$E_m(\omega) = E_m^+(\omega)e^{ikz} + E_m^-(\omega)e^{-ikz}, \tag{2.29}$$

where z is bounded within the region of interest. The amplitude of the electric field at that exact location is just the summation of the two terms

$$E_m(\omega) = E_m^+(\omega) + E_m^-(\omega). \tag{2.30}$$

2.2.3 E-Field in Time Domain

Extending this model into the time domain is fairly straightforward. Assume you have an input field as a function of time $E_{Input} = E_{Input}(t)$. The algorithm to handle this sort of field is simply to take the fourier transform of this field

$$\hat{E}_{Input}(\omega) = \int_{-\infty}^{\infty} e^{i\omega t} E_{Input}(t)dt, \tag{2.31}$$

and handle it in frequency space as shown in the previous sections. Once you transform the field in frequency space both solving for the overall configuration and propagating the array to the point of interest, you would go back into the time domain using the inverse fourier transform only now you will have two terms. One for the forward propagating waves and a second for the backwards propagating waves. Using equation 2.30 we obtain the relation

$$\boxed{\hat{E}_m(t) = \frac{1}{2\pi}\int_{-\infty}^{\infty} e^{-i\omega t}[E_m^+(\omega) + E_m^-(\omega)]dt} \tag{2.32}$$

which allows one to determine the electric field, as a function of time, at an arbitrary location in the optical configuration.

2.3 Working Model for the Microcavity

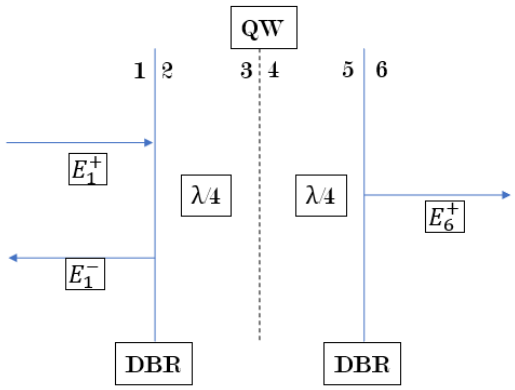

Figure 2.1: Working diagram of the cavity. This generalizes each region with labels to do some preliminary investigations. A working theoretical model is created out of these labels. The multilayer DBRs are symbolically represented by a single interface. It should be noted that there is no left propagating light on the right side of the cavity as we are limiting ourselves to only having incoming light in a single direction. The subscripts of the E-Field denote which region they represent.

2.3.1 Field in the Various Regions

In the following section, the overarching problem of the thesis will be proposed. Essentially we are interested in determining the electric field at the quantum well. Previous phenomenological models are to be replaced with a new integral obtained from the methods proposed in this thesis. Figure 2.1 shows a working diagram of the cavity that will be used for the derivations to follow. Using the proposed transfer matrix method from the previous section, one can deduce the field driving the quantum well. Assume you begin with an input spectrum $E_{inp}(\omega)$ and a total matrix $M^{total}(\omega)$. You would setup the array

$$\begin{pmatrix} E_1^+(\omega) \\ E_1^-(\omega) \end{pmatrix} = \begin{pmatrix} E_{inp}(\omega) \\ -\frac{M_{21}^{total}(\omega)}{M_{22}^{total}(\omega)} E_{inp}(\omega) \end{pmatrix}, \tag{2.33}$$

where the subscripts for $E_1^+(\omega)$ and $E_1^-(\omega)$ refer to the region (region 1 in this case) in the Figure 2.1 and the hyperscripts denote the foward (+) propagating and backward (-) propagating light. Here M^{total} is the total matrix that models the cavity. It is built evaluating

$$M^{total} = M_{DBR} M_{\lambda/4} M_{QW} M_{\lambda/4} M_{DBR}. \tag{2.34}$$

M_{DBR} is a product of matrices alternating between an interface and propagation matrix, $M_{\lambda/4}$ is a propagation matrix that propagates the field over a resonant $\lambda/4$ layer, and M_{QW} is the quantum well matrix deduced in the previous sections. The exact construction of each of these matrices can be found in earlier sections. These matrices model exactly how the electric field transforms as it propagates through the cavity. The field at the quantum well is then

$$E_{QW} = E_3^+ + E_3^-. \tag{2.35}$$

It should be noted that we are assuming the quantum well to be infinitely thin (and therefore 2 dimensional) and the field in region 3 (after propagation to the quantum well) to be the field at the quantum well. We introduce two new matrices in order to simplify our calculations

$$\begin{aligned} M^L &= M_{\lambda/4} M_{DBR} \\ M^R &= M_{DBR} M_{\lambda/4} \\ M^{cavity} &= M^R M^L, \end{aligned} \tag{2.36}$$

where M^R is a matrix representing everything to the right of the quantum well, M^L represents everything to the left, and M^{cavity} is a matrix that represents the full cavity without the quantum well. Propagating our field in region 1 to region 3 gives us

$$\begin{pmatrix} E_3^+(\omega) \\ E_3^-(\omega) \end{pmatrix} = M^L \begin{pmatrix} E_1^+(\omega) \\ E_1^-(\omega) \end{pmatrix}. \tag{2.37}$$

To get the field in region 4, you would then apply a quantum well matrix. The polarization term induced by the quantum well is left written explicitly so as to see how the polarization affects the field at the quantum well. The polarization is of interest to us so for that reason we extract out the polarization term. The field in region 4 is then

$$\begin{aligned} \begin{pmatrix} E_4^+(\omega) \\ E_4^-(\omega) \end{pmatrix} &= \left[\begin{pmatrix} 1 & 0 \\ 0 & 1 \end{pmatrix} + 2\pi i \frac{\omega_p}{c_0 n \cos\theta} \chi(\omega p) \begin{pmatrix} 1 & 1 \\ -1 & -1 \end{pmatrix} \right] \begin{pmatrix} E_3^+(\omega) \\ E_3^-(\omega) \end{pmatrix} \\ \begin{pmatrix} E_4^+(\omega) \\ E_4^-(\omega) \end{pmatrix} &= \begin{pmatrix} 1 & 0 \\ 0 & 1 \end{pmatrix} \begin{pmatrix} E_3^+(\omega) \\ E_3^-(\omega) \end{pmatrix} + 2\pi i \frac{\omega_p}{c_0 n} \chi(\omega) \begin{pmatrix} 1 & 1 \\ -1 & -1 \end{pmatrix} \begin{pmatrix} E_3^+(\omega) \\ E_3^-(\omega) \end{pmatrix} \\ \begin{pmatrix} E_4^+(\omega) \\ E_4^-(\omega) \end{pmatrix} &= \begin{pmatrix} E_3^+(\omega) \\ E_3^-(\omega) \end{pmatrix} + 2\pi i \frac{\omega_p}{c_0 n} \begin{pmatrix} 1 \\ -1 \end{pmatrix} P_{QW}(\omega), \end{aligned} \tag{2.38}$$

where the polarization is just

$$P_{QW}(\omega) = \chi(\omega)(E_3^+ + E_3^-). \tag{2.39}$$

The field in region 6 is

$$\begin{pmatrix} E_6^+(\omega) \\ E_6^-(\omega) \end{pmatrix} = M^R \begin{pmatrix} E_4^+(\omega) \\ E_4^-(\omega) \end{pmatrix}, \tag{2.40}$$

which we limit ourselves to the usual case in which the light in region 6 is completely forward traveling (no input light from the right of the cavity). The field in region 6 can then be written as

$$\begin{aligned} \begin{pmatrix} E_6^+(\omega) \\ 0 \end{pmatrix} &= M^R M^L \begin{pmatrix} E_1^+(\omega) \\ E_1^-(\omega) \end{pmatrix} + M^R 2\pi i \frac{\omega_p}{c_0 n} \begin{pmatrix} 1 \\ -1 \end{pmatrix} P_{QW}(\omega) \\ \begin{pmatrix} E_6^+(\omega) \\ 0 \end{pmatrix} &= M^{cavity} \begin{pmatrix} E_1^+(\omega) \\ E_1^-(\omega) \end{pmatrix} + M^R 2\pi i \frac{\omega_p}{c_0 n} \begin{pmatrix} 1 \\ -1 \end{pmatrix} P_{QW}(\omega). \end{aligned} \tag{2.41}$$

This gives us the system of equations we've seen previously only written out. If we define the second term to be

$$\begin{pmatrix} I_1 \\ I_2 \end{pmatrix} = M^R 2\pi i \frac{\omega_p}{c_0 n} \begin{pmatrix} 1 \\ -1 \end{pmatrix} P_{QW}(\omega), \tag{2.42}$$

we can solve for the field in region 1

$$E_1^- = -\frac{M_{21}^{cavity}}{M_{22}^{cavity}} E_1^+ - \frac{I_2}{M_{22}^{cavity}}, \tag{2.43}$$

which then in terms of the input field is just

$$\boxed{E_1^- = -\frac{M_{21}^{cavity}}{M_{22}^{cavity}} E_{inp} - \frac{I_2}{M_{22}^{cavity}}} \tag{2.44}$$

2.3.2 Field at the Quantum Well

Using equations 2.35, 2.37, and 2.43 we get

$$\begin{aligned}
E_{QW} &= M_{11}^L E_1^+ + M_{12}^L E_1^- + M_{21}^L E_1^+ + M_{22}^L E_1^- \\
E_{QW} &= (M_{11}^L + M_{21}^L) E_1^+ + (M_{22}^L + M_{12}^L) E_1^- \\
E_{QW} &= (M_{11}^L + M_{21}^L) E_1^+ - (M_{22}^L + M_{12}^L)(\frac{M_{21}^{cavity}}{M_{22}^{cavity}} E_1^+ + \frac{I_2}{M_{22}^{cavity}} \\
E_{QW} &= (M_{11}^L + M_{21}^L) - (M_{22}^L + M_{12}^L)\frac{M_{21}^{cavity}}{M_{22}^{cavity}}) E_1^+ \\
&\quad - \frac{(M_{22}^L + M_{12}^L)}{M_{22}^{cavity}} (M_{21}^R - M_{22}^R) 2\pi i \frac{\omega_p}{c_0 n} P_{QW}.
\end{aligned} \tag{2.45}$$

To shorten the expression we make the definition

$$\begin{aligned}
a(\omega) &= (M_{11}^L + M_{21}^L) - (M_{22}^L + M_{12}^L)\frac{M_{21}^{cavity}}{M_{22}^{cavity}} \\
b(\omega) &= -\frac{(M_{22}^L + M_{12}^L)}{M_{22}^{cavity}} (M_{21}^R - M_{22}^R) 2\pi i \frac{\omega_p}{c_0 n},
\end{aligned} \tag{2.46}$$

which allows to neatly relate the field at the quantum well to the polarization and the input electric field. The relation is

$$E_{QW}(\omega) = a(\omega) E_{inp}(\omega) + b(\omega) P_{QW}(\omega). \tag{2.47}$$

and finally in the time domain, the field at the quantum well becomes

$$E_{QW}(t) = \frac{1}{2\pi} \int_{-\infty}^{\infty} e^{-i\omega t} [a(\omega) E_{inp}^+(\omega) + b(\omega) P_{QW}(\omega)] dt. \tag{2.48}$$

The fourier transform can then be evaluated using this convolution integral via the convolution theorem

$$E_{QW}(t) = \int_{-\infty}^{\infty} \hat{a}(t - t') E_{inp}^+(t') + \hat{b}(t - t') P_{QW}(t') dt. \tag{2.49}$$

The question being tackled in this project is finally whether or not it is valid to bound the integral so that we integrate from $t' = -\infty$ to $t' = t$ so that $E_{QW}(t)$ is retarded with respect to the input light $E_{inp}(t')$ and $P_{QW}(t')$

$$\boxed{E_{QW}(t) = \int_{-\infty}^{t} A(t - t') E_{inp}^+(t') + B(t - t') P_{QW}(t') dt} \tag{2.50}$$

where we defined A and B by this integral

$$A(t-t') = \int_{\omega_{min}}^{\omega_{max}} \frac{d\omega}{2\pi} a(\omega) e^{-i\omega(t-t')}. \tag{2.51}$$

which will then allow for a more thorough expression for the time derivative of the electric field at the quantum well. This new defintion adds bounds to the frequncies used in the limits of integration and therefore is not exactly a fourier transform. Section 5 will elaborate more on this response function and its behaviors.

3 The Microcavity

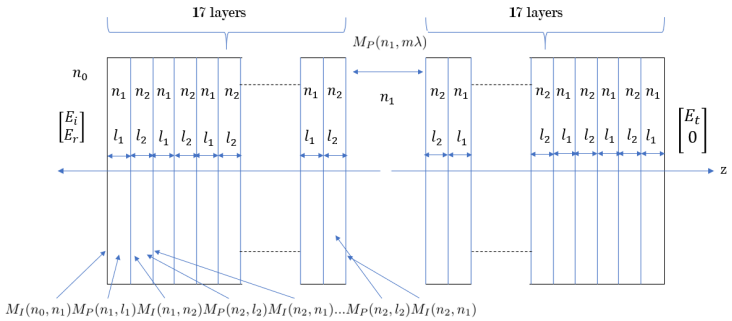

Figure 3.1: Diagram of cavity without the quantum well. This figure adds more detail than the previous figure of the cavity being modeled. Although the quantum well is not included in this setup, the details of the DBRs are demonstrated here. A layer is actually a pair of two layers which together make a couple. There are 17 of those (or 35 actual slabs/layers if you count the layer in between). The matrix below the first DBR demonstrates the nature of the matrices that build the total matrix that represents the DBR. The second DBR has a similar matrix to represent its structure. The dots in between the layers of each DBR signify that there are more repetitive layers not shown explicitly.

3.1 The Cavity without QW

Below are some results when the transfer matrix method is applied to a pair of DBR mirrors that form an empty cavity. Each DBR is made of 17 coupled layers alternating between a medium with index $n_1 = 3.1$, an index of $n_2 = 3.6$. A final layer is placed at the end of each cavity of index n_1 so that these ends are facing each other. In this section we will be varying this length as it is what forms the medium surrounding the quantum well in the true setup. The thickness of the layers are $l_i = (\pi\hbar c_0)/(2n_i E_{res})$ which correspond to $\lambda/4$ layers with the resonant energy set to $E_{res} = 1.599meV$. On the incident side we have an index of $n_0 = 1$ and on the transmitted side we have an index of $n_4 = 3$. The area between the cavity is just n_1. Figure 3.1 shows the setup along with the matrices that will be used to model the DBRs. We use the following relations and matrices to compute the various fields assuming normal incidence and TE light:

$$M_I(n_1, n_2) = \frac{1}{2n_2}\begin{pmatrix} n_2 + n_1 & n_1 - n_2 \\ n_1 - n_2 & n_2 + n_1 \end{pmatrix} \tag{3.1}$$

$$M_P(\omega_p, n_i, l_i) = \begin{pmatrix} e^{i\frac{\omega_p n_i}{c_0} l_i} & 0 \\ 0 & e^{-i\frac{\omega_p n_i}{c_0} l_i} \end{pmatrix} \tag{3.2}$$

$$\begin{pmatrix} E_t \\ 0 \end{pmatrix} = M_{total} \begin{pmatrix} E_i \\ E_r \end{pmatrix}. \tag{3.3}$$

These equations relate the input field to the resultant field using the matrices for propagation and refraction/reflection. The total matrix will include two DBR matrices. The DBR matrices will be

$$\begin{aligned} M_{DBR1} &= M_I(n_2, n_1)M_P(n_2, l_2)...M_P(n_2, l_2)M_I(n_1, n_2)M_P(n_1, l_1)M_I(n_0, n_1) \\ M_{DBR2} &= M_I(n_1, n_4)M_P(n_1, l_1)...M_P(n_1, l_1)M_I(n_2, n_1)M_P(n_2, l_2)M_I(n_1, n_2). \end{aligned} \tag{3.4}$$

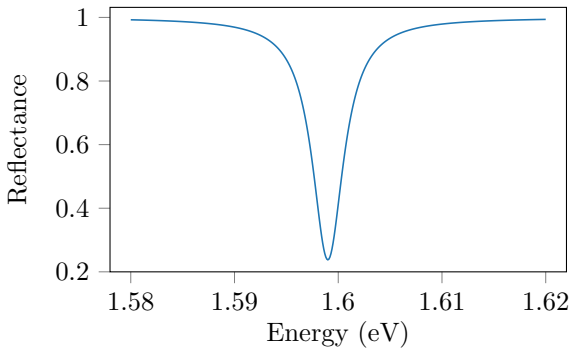

Figure 3.2: Here we have a reflectance profile of a pair of DBRs. The resonance coincides with the thickness of the alternating layers but also the separation of the DBRs. The x-axis is corresponding to frequencies of light with that particular energy. The broadness can be attributed to the seperation of the two DBRs. It should be noted that at resonance, the cavity resorts to the natural reflectance of 0.25 which corresponds from the reflection between a medium with index $n_1 = 1.0$ and $n_2 = 3.0$. This is the profile of the cavity before the quantum well is inserted.

Referring back to figure 3.1, the matrices transform the array as the light experiences each obstacle. In the equation, the terms are aligned so that you have the light to the far right of the relation and then to its immediate left, the first obstacle (in this case $M_I(n_0, n_1)$) and then the next one following that one. The expression written out is

$$\begin{pmatrix} 1 \\ 0 \end{pmatrix} = M_{DBR2} M_P(n_1, m\lambda/2) M_{DBR1} \begin{pmatrix} \frac{E_i}{E_t} \\ \frac{E_r}{E_t} \end{pmatrix}, \tag{3.5}$$

where $\lambda = (hc_0)/E_{res}$ which is the wavelength of light in a vacuum associated with the resonant energy.

3.1.1 Reflectance and E-field

Using this model we can deduce some behaviors of the cavity one of those being the distance between the DBR's affects the reflectances of the cavity. Since in this setup, the layers of the DBR correspond to the same wavelength used to calculate the seperation, you expect certain behaviors. If say the separation between the DBRs is $m\lambda = (50/2)\lambda$ you get a sharp resonance at the corresponding energy (1.599 meV) as shown in Figure 3.3a. If we use $m\lambda = \lambda/2$ then we get a broader dip in the reflectance as seen in Figure 3.2. Figure 3.3b shows the case where the separation is no longer a multiple of $\lambda/2$. This shows that the separation is crucial in determining the modes the cavity is able to support.

Another bit of information was extracted in order to further investigate the cavity without the quantum well. Simulations were done to determine the electric field amplitude at each boundary. Figure 3.4 shows the case in which the incoming light is resonant and the case in which it is not. These are monochromatic fields and only information regarding the amplitudes are shown. As expected, the resonant light was amplified at the center of the cavity due to the nature of the cavity. The light becomes trapped and constructively interferes to create a large amplitude between the DBRs. The off resonant light does not exhibit this behavior as most of the light just gets reflected and escapes the cavity.

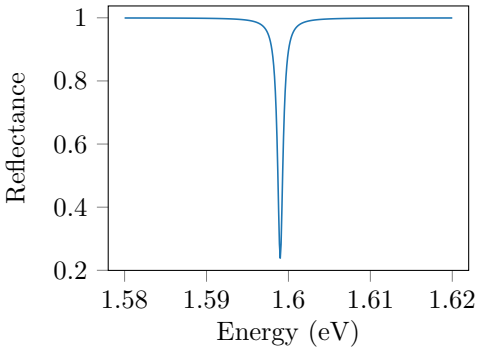

(a) when seperation is large

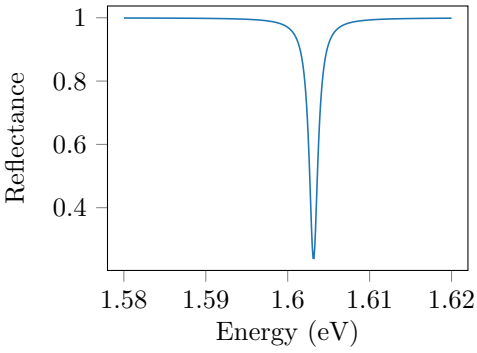

(b) when seperation is off resonance

Figure 3.3: We demonstrate other behaviors of our cavity in these figures. The left figure shows that at larger separations, keeping the separation a multiple of the resonant wavelength, causes the dip to be much sharper as it is harder for off resonant light to survive in this cavity. The right shows what happens when we set an arbitrary seperation. The resonance shifts accordingly to represent the new mode its able to support

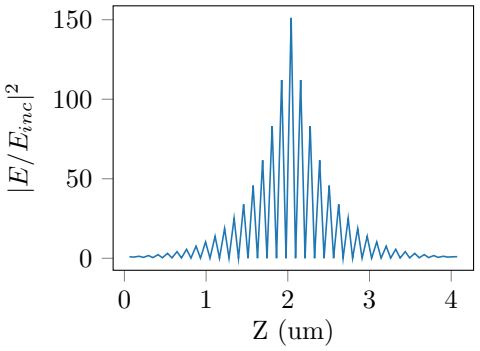

(a) Resonant light

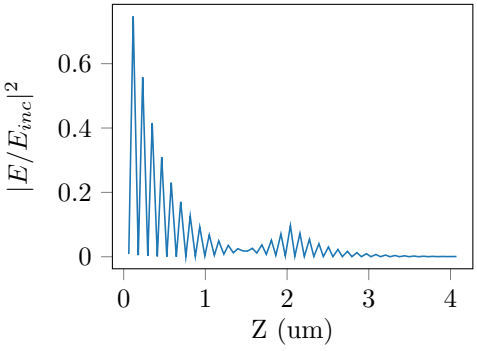

(b) Off resonant light

Figure 3.4: These figures show how the amplitude of the electric field varies through the cavity in the case that the cavity is seperated by two $\lambda/4$ layers. This is therefore the setup of the cavity being used throughout the rest of the investigation. For now the quantum well is excluded though. The field amplitude was divided by the amplitude of the incoming light and squared so as to show a relative field strength and to be able to compare both cases. The plots have a data point for every interface in the cavity. At one layer you have some stable level of light and then at the interface for the next layer a standing wave node

3.2 Cavity with the Quantum Well

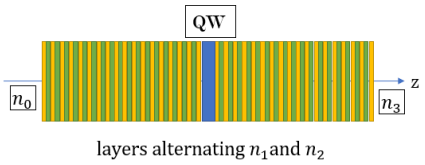

Figure 3.5: Diagram of the cavity with quantum well. At this point, we finally introduce the quantum well in the setup. It should be noted that the actual quantum well is assumed to have zero thickness which makes this diagram a bit misleading. The DBRs are of the same structure presented previously with alternating indices and 17 coupled layers.

3.2.1 Evaluating the Quantum Well Matrix

The next step is to introduce the quantum well into the cavity. The DBR's are set exactly $\lambda/2$ apart (each DBR has a $\lambda/4$ layer at their ends) and the quantum well is directly between them. The quantum well is defined to be infinitesimal and so is only modeled with one matrix. Using the quantum well matrix, we model its response to the incoming light. We limit ourselves to (TE) light and normal incidence.

$$M_{QW}^{TE}(n,\omega_p) = \begin{pmatrix} 1 & 0 \\ 0 & 1 \end{pmatrix} + 2\pi i \frac{\omega_p}{c_0 n}\chi(\omega_p)\begin{pmatrix} 1 & 1 \\ -1 & -1 \end{pmatrix}, \tag{3.6}$$

where χ is of course

$$\chi(\omega) = -|\vec{d}|^2 \frac{|\Omega_{ls}(r=0)|^2}{\hbar\omega - \varepsilon_x + i\gamma x}. \tag{3.7}$$

The values set for the various constants were as follows. The electric dipole moment was set to $e < c|\vec{r}|v >= 10e\mathring{A}$, the bohr radius $a_0 = 170\mathring{A}$, the resonant energy (which was set to be the exciton resonant energy) $\varepsilon_x = 1.601eV$, and the dephasing rate $\gamma_x = 0.0002eV$. The index was set to $n = 3.1$ corresponding to the surrounding medium. The $\hbar\omega$ corresponds to the energy associated with the input field. Evaluating the susceptibility term gives us

$$\begin{aligned} \chi &= -|10e\mathring{A}|^2 |\frac{2\sqrt{2}}{170\mathring{A}\sqrt{\pi}}|^2 \frac{1}{\hbar\omega - 1.601eV + 0.0002eV} \\ \chi &= -(\frac{800}{170^2\pi})(\frac{e^2}{\hbar\omega - 1.601eV + 0.0002eV}). \end{aligned} \tag{3.8}$$

3.2.2 Reflectance and E-Field Amplitude in Spatial Domain

Adding this matrix in between the two DBRs causes the resonance to split into two. Originally the cavity had a reflectance dip centered around $1.599eV$ corresponding to the resonance of the DBRs. The reflectance with the added quantum well shown in figure 3.6 demonstrates energy dips at two different energy levels. The are approximately $1.594eV$ and $1.606eV$ corresponding to a lower polariton (LP) and upper polariton (UP) resonance.

After approximating these new resonances, monochromatic light corresponding to those energies were simulated as they went through the cavity. Figure 3.7 demonstrates what the field amplitudes look like in the spatial domain. This rudimentary model shows that with the added quantum well we get huge spikes in

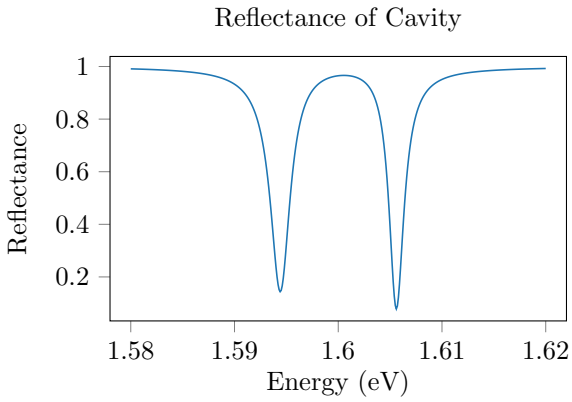

Figure 3.6: Reflectance of the total cavity. This is a comparable figure to 3.2 in the sense that it demonstrates exactly what happens after the quantum well is introduced. The resonance splits into two resonances with one being the lower polariton (LP) and the other the upper polariton (UP) resonances. It should be noted that there is some structure to this resonance beyond this range of energy levels but these are the ones of interest. Later on, to perform various calculations, a much larger domain must be used.

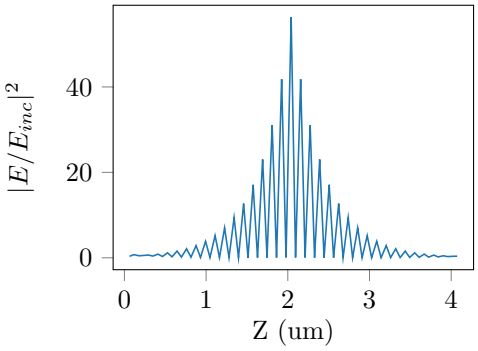

(a) Lower polariton field propagation

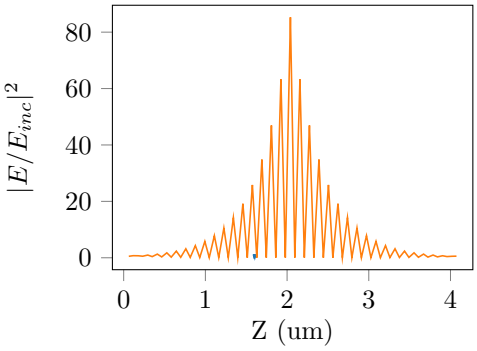

(b) Upper polariton field propagation

Figure 3.7: The propagation of the E-field amplitude is demonstrated in these figures. The behavior is very similar to the case without the quantum well where resonant light gets amplified at the center of the cavity. Again, the plots have a data point for every interface in the cavity. At one layer you have some stable level of light and then at the interface for the next layer a standing wave node.

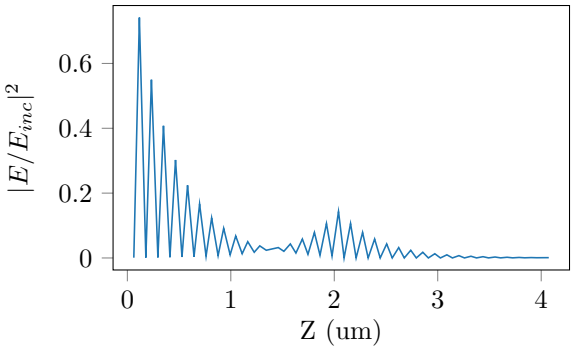

Figure 3.8: Off resonant light was used as a means to make sure the simulated model was working as it should. This behavior is what was expected and so this gives a certain amount of assurance to the results. Much like the off resonant no quantum well case in the previous section, the amplitude of the field quickly dies out as the off resonant field is highly reflective and so the resonator will not sustain this frequency of light.

the amplitude. This gives us an idea of what we are to expect of the electric field when we determine the field in the frequency and temporal domain. Off resonant light was also modeled in figure 3.8 as a reference to demonstrate the behavior of the newly formed cavity. Adjustments will be made later for the detuning when demonstrating the resolved field using the bounded integral.

3.3 Propagation of a Gaussian Pulse

3.3.1 Pulse Shape

Using a pulse as the incoming light is a means to making sure the model for the cavity is working properly. Per usual, we expect certain behavior as the pulse is propagated through the cavity. The very first of which we expect to have a delay in the pulse in the time domain. If the initial pulse is centered about the origin in the time domain, the pulse after propagation should be centered at a later time. This time, of course, being the time of flight it takes light to reach the center of the cavity. It should be noted that the time width needs to be narrow enough to be able to resolve this effect, otherwise there will be too much overlap between the pulse and its reflections. We expect that at resonance, the peak power of the pulse increases as seen with a resonant incoming electric field. The Gaussian pulse that was used is

$$E_{inp}(\omega) = E_0[e^{-(\frac{(\omega-\omega_{res})}{\sigma_\omega})^2} + e^{-(\frac{(\omega+\omega_{res})}{\sigma_\omega})^2}], \tag{3.9}$$

where ω is the frequency of the incoming light, ω_{res} is a frequency resonant with the cavity (which also serves as where the Gaussian will be centered over), and σ_ω is directly proportional to the spectral width of the Gaussian. It should be noted that two gaussians are being used to model the negative and positive frequencies so that the fourier transform is properly handled. Negative frequencies were included as well just for the sake of this test. The RMS width (found in the appendices of [11]) in the time domain in terms of the RMS width in the frequency domain is simply

$$\sigma_t = \frac{1}{\sigma_\omega}. \tag{3.10}$$

3.3.2 Short Pulse and Time of Flight

The first gaussian that was propagated through the cavity using the fourier methods previously described was a broad Gaussian in frequency domain. The idea is to get a short pulse in the time domain so that the peaks of field in both the incident field and at the quantum well can be resolved. The time of flight of the pulse can then be tested to make sure that it agrees with analytical results. Using the fact that the propagation distance is a sum of the thickness of each layer of the DBRs in which each individual layer is $l_i = (\pi\hbar c_0)/(2n_i 1.599eV)$, the phase velocity in each medium is $\nu = c_0/n$, and the relation between distance, velocity, and time is $v = d/t$, the time t it takes for the light to propagate through cavity and arrive at the quantum well is

$$t = \sum_{i=1}^{35} \frac{\pi\hbar}{2 * 1.599eV} \approx 22.63fs. \tag{3.11}$$

Note that there are 35 layers here which correspond to the 17 coupled layers of the first DBR and the $\lambda/2$ layer in the center. One of the resonant energies of the cavity was used arbitrarily. Note that this is the resonance corresponding to the cavity and not the resonance used to construct the DBRs. σ_f is chosen such that the corresponding RMS width in the time domain is much smaller than the time of flight. A $\sigma_t = 1fs$ was arbitrarily chosen. The results can be seen in figure 3.9. The time different between the two peaks was found to be $\Delta t \approx 22.75fs$. The reason for the discrepancy is the resolution used in the time domain was not fine enough to resolve $0.01fs$. This would require much more sampling points and a much longer run time. Regardless this should suffice. Another thing to note about the figure is the amplitude of the pulse diminishing which is simply due to the fact that most of the frequencies utilized were not useful and far from resonant.

3.3.3 Narrow Bandwidth pulse

For the sake of being thorough, the same simulation was done for a much broader pulse with the expectation of finding an amplification in the amplitude. It is much more difficult to resolve the different pulses in the

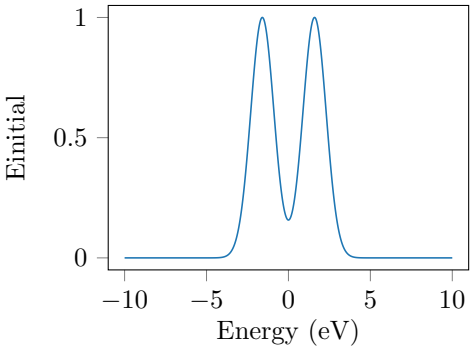

(a) Energy spectrum of broad gaussian

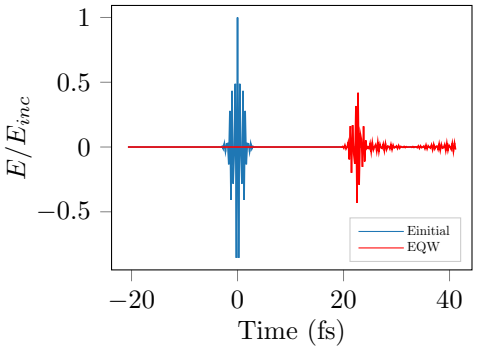

(b) Broad gaussian pulse in time domain

Figure 3.9: This figure shows the first attempts at finally doing something meaningful with our simulations. The behaviors of injecting a gaussian pulse into the cavity were deduced by our models and shown here. A broad gaussian was used so that the corresponding pulse in the time domain would be sharper and easier to resolve its peaks. This is also to reduce the overlap as the pulse needed to be shorter than the actual cavity. The left graph shows the frequency spectrum of the incoming light and the right shows the incoming pulse followed by the pulse once it reaches the quantum well. The peaks were resolved and the time difference calculated to make sure the time difference agrees with the time of flight calculated. These fields were not squared however, like previous amplitude models, so as to show the negative oscillations in the figures.

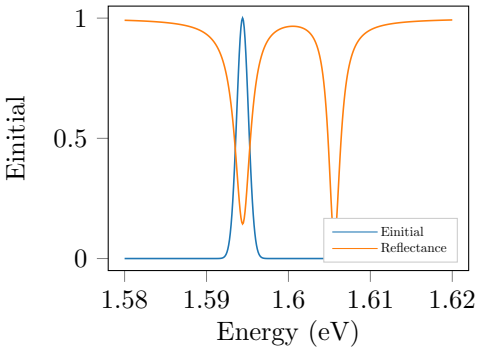

(a) Energy spectrum of narrow gaussian

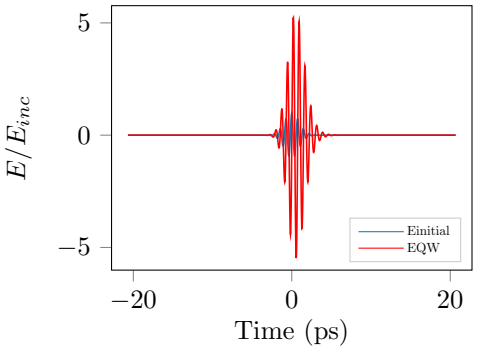

(b) Narrow gaussian pulse in the time domain

Figure 3.10: As opposed to the previous gaussian use, this one is much more narrow in the frequency domain which leads to a much broader pusle in the time domain. The extreme amount of overlap in the time domain is due to that fact. The field in the time domain is plotted as a relative strength to the incoming light. These fields were not squared, like previous amplitude models, however so as to show the negative oscillations in the figures. Ultimately, we are interested in the e-field at the quantum well so we want to see these oscillations as well.

time domain when you have a narrow bandwidth as there is a lot of interaction between the pulse and its reflections. As noted before, it takes roughly $22.63fs$ for a pulse to propagate to the center of the cavity. If we choose a σ_t that is a couple of multiples larger than that, then there will be alot of overlap with the pulse as it propagates. Figure 3.10 shows how much overlap there is in the time domain. The RMS width in the time domain σ_t was set to be $0.93ps$. This allows for the pulse to overlap multiple times over itself. Since this is a broad signal in the time domain, it is narrow around the resonance which allows it to be amplified by the cavity. The pulse peak magnifies 5 times that of the incident pulse.

4 Testing and Debugging

4.1 Dielectric Slab

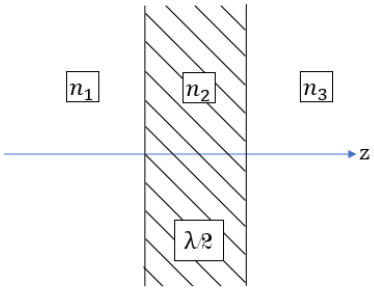

Figure 4.1: Diagram of the dielectric slab. The indices are labeled so as to coincide with the derivations in the section.

The dielectric slab is a very straightforward optical setup. It has been thoroughly investigated and as such it is a great way to test to make sure that the working model for the overall cavity is sufficient. It tests the very basics of the model which are the propagation and interface matrices.

4.1.1 Setting Up The Matrices

Per usual we use the following relationship to relate the incident, reflected, and trasmitted fields

$$\begin{pmatrix} E_i \\ E_r \end{pmatrix} = M^{TE}_{Dielectric} \begin{pmatrix} E_t \\ 0 \end{pmatrix}, \tag{4.1}$$

and use the following two transformation matrices to model what happens during propagation and when the light hits an interface within the dielectric slab

$$M_P = \begin{pmatrix} e^{i\frac{\omega_p n_2}{c_0}\Delta z} & 0 \\ 0 & e^{-i\frac{\omega_p n_2}{c_0}\Delta z} \end{pmatrix}, \tag{4.2}$$

$$M_I = \frac{1}{2n_2}\begin{pmatrix} n_2+n_1 & n_1-n_2 \\ n_1-n_2 & n_2+n_1 \end{pmatrix}. \tag{4.3}$$

The slab has 3 areas. The left, middle, and right region. The left and right region are in air so $n_1 = 1.0$. These regions however wont produce a significant phase factor (at least pertaining to intensities). The term will get cancelled out. The siginificant matrices are then the ones that relate field immediately before and after the dielectric slab, which when applied to equation (4.1) takes the following form:

$$\begin{pmatrix} E_i \\ E_r \end{pmatrix} = M_I M_P M_I \begin{pmatrix} E_0 e^{ikz} \\ 0 \end{pmatrix} \tag{4.4}$$

which interprets as being an entrance interface, propagation, and then an exit interface between the transmitted field and the incident/reflected fields. It should be noted that now we are propagating the output field to the incident field. This relation can be expressed either way and produce the same results but with some configurations, it is much more convenient to have it one way over the other.

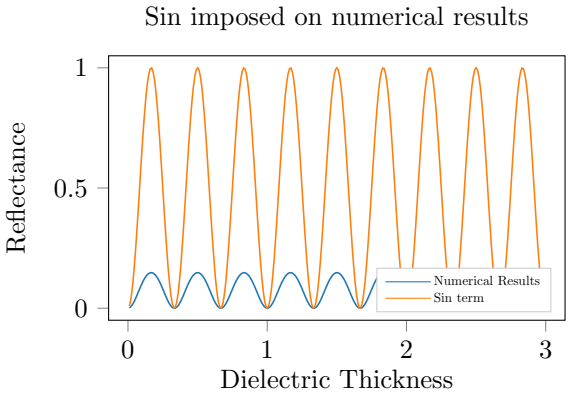

Figure 4.2: Gamma Term superimposed on the numerical results so as to demonstrate that our numerical results are mode spaced as they should be. The actual amplitudes are not significant as we are only trying to demonstrate mode spacing. It would also prove difficult to resolve if the amplitudes were the same as they would completely overlap.

4.1.2 Computing Reflectance and Mode Spacing

Now to deduce the shape of the reflectance analytically, we make a substitution for the sake of brevity in our algebra. Allow $\Gamma = \frac{\omega_p n_2}{c_0}\Delta z$ and then you get the following:

$$
\begin{aligned}
\|E_i\|^2 &= \|(n_2+n_1)^2 e^{i\Gamma} + (n_1-n_2)(n_2-n_1)e^{-i\Gamma}\|^2 \\
\|E_i\|^2 &= \|(n_2+n_1)^2 e^{i\Gamma} - (n_2-n_1)^2 e^{-i\Gamma}\|^2 \\
\|E_i\|^2 &= (n_2+n_1)^4 - (n_2-n_1)^2(n_2+n_1)^2(e^{i2\Gamma}+e^{-i2\Gamma}) + (n_2-n_1)^4 \\
\|E_i\|^2 &= (n_2+n_1)^4 - 2(n_2-n_1)^2(n_2+n_1)^2(\cos 2\Gamma) + (n_2-n_1)^4 \\
\|E_r\|^2 &= \|(n_2+n_1)(n_1-n_2)e^{i\Gamma} + (n_1+n_2)(n_2-n_1)e^{-i\Gamma}\|^2 \\
\|E_r\|^2 &= \|(n_2+n_1)(n_1-n_2)(e^{i\Gamma}-e^{-i\Gamma})\|^2 \\
\|E_r\|^2 &= \|2i(n_2+n_1)(n_1-n_2)(\sin\Gamma)\|^2 \\
\|E_r\|^2 &= 4(n_1^2-n_2^2)^2(\sin^2\Gamma) \\
\frac{\|E_r\|^2}{\|E_i\|^2} &= \frac{4(n_1^2-n_2^2)^2(\sin^2\Gamma)}{(n_2+n_1)^4 - 2(n_2-n_1)^2(n_2+n_1)^2(\cos 2\Gamma) + (n_2-n_1)^4} \\
\frac{\|E_r\|^2}{\|E_i\|^2} &= \frac{A(\sin^2\Gamma)}{-B(\cos 2\Gamma)+C}.
\end{aligned}
\tag{4.5}
$$

In the final line, the index terms were replaced with constants to better show the behavior of the function. This result means that the reflectance is therefore related to a $\sin^2\Gamma$ term (and inversely to a $\cos 2\Gamma$ term). We can expect maximums whenever $\Gamma = \frac{\pi m}{2}$ or $\omega_p = \frac{\pi m c_0}{2n_2\Delta_z}$ where m is an integer. This defines the spacings of the modes with m as our label for each mode. Below is this $\sin^2\Gamma$ term super imposed on the numerical results as a means to verify the result.

4.1.3 Comparing Results

The configurations were compared to the literature. In [2] there is a graph showing the reflectances for various index configurations. In Figure 4.3 we compare the results between what was obtained through simulations and the literature.

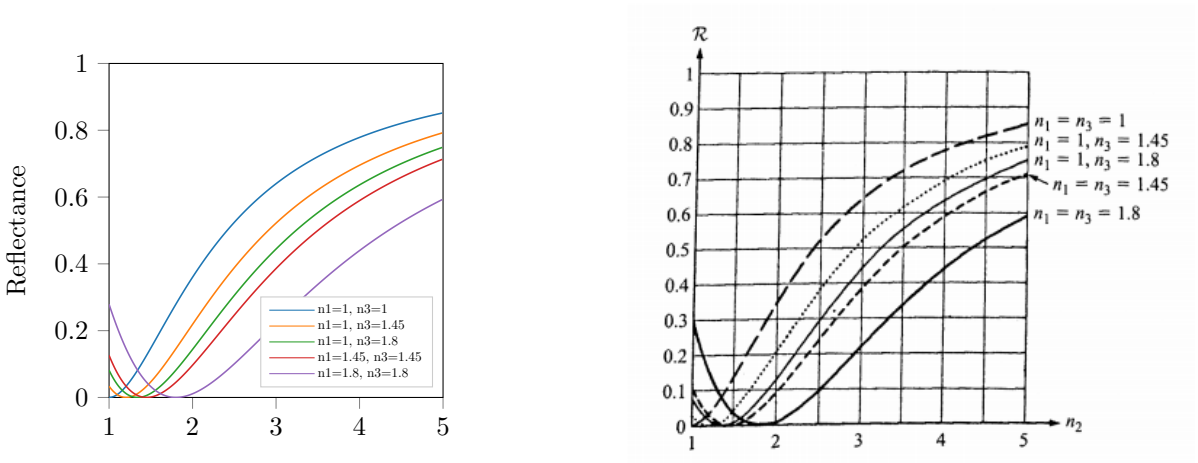

Figure 4.3: The results obtained numerically are compared to the literature. It should be obvious which bands correspond to each other between the two graphs but a legend was provided to avoid confusion. Some deformation may be witnessed due to scaling and such but the results were also compared numerically just to confirm that they are in fact the same.

4.2 DBR Mirrors

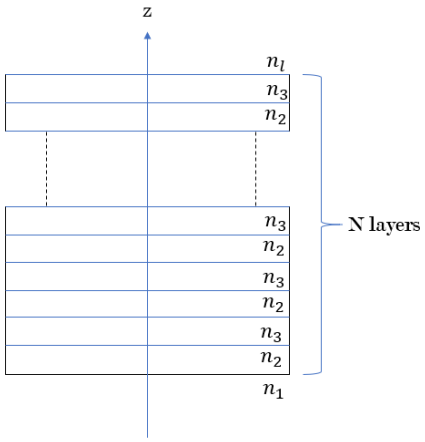

Figure 4.4: Diagram of the DBR. The dots are there to represent any arbitrary number of layers. This diagram very much coincides to the diagram used in the earlier sections to demonstrate the cavity so as to keep the same conventions. In this case however, we manipulate the number of layers.

One effective test is to make sure the setup of the DBR mirrors agrees with the literature in regards to the reflectances. The diagram shown in figure 4.4 shows the setup of the DBR's and has a corresponding equation for the reflectance

$$R_{2N} = \left(\frac{1 - \frac{n_l}{n_1}(\frac{n_2}{n_3})^{2N}}{1 + \frac{n_l}{n_1}(\frac{n_2}{n_3})^{2N}} \right)^2, \tag{4.6}$$

which is taken from [2]. Here, the indices correspond to the figure and thus $n_l = 3.0$, $n_2 = 3.1$,$n_3 = 3.6$, and $n_1 = 1.0$. The DBR's in the cavity being modeled have 17 coupled layers if you exclude the layer that is in contact with the QW. Evaluating the expression gives

$$R_{2N} = \left(\frac{1 - \frac{3.0}{1.0}(\frac{3.1}{3.6})^{34}}{1 + \frac{3.0}{1.0}(\frac{3.1}{3.6})^{34}} \right)^2 \approx 0.9284. \tag{4.7}$$

which is in agreement with our simulations. To demonstrate this, the reflectance was plotted as a function of the number of layers. Figure 4.5 shows the reflectances. The results obtained through the simulation model were artificially shifted up so as to compare the results. The RMS error between the two results was $\approx 7.7E-16$. This quantity is

$$Error = \sqrt{\sum_{i=0}^{N} \frac{(R_i^{born} - R_i^{num})^2}{N-1}}, \tag{4.8}$$

where R^{born} is the reflectance as given by born and R^{num} is from numerical results.

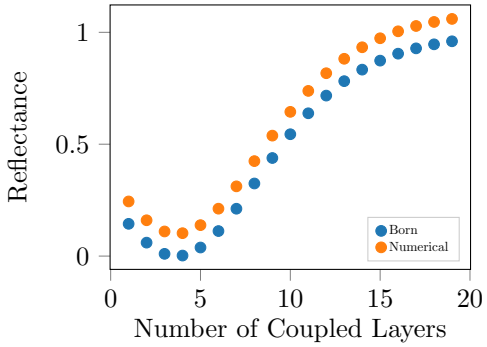

Figure 4.5: This shows the reflectances obtained through numerical simulations and from the literature. The results are artificially shifted by 0.1 to show that they have the same shape. The x-axis is the amount of coupled layers not to be confused with actual layers as each coupled layers counts for 2 different index layers.

4.3 Single Layer Test

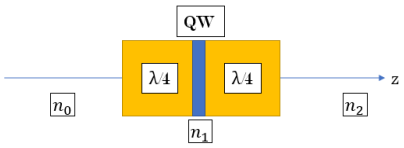

Figure 4.6: Diagram of the single layer setup. The figure demonstrates the convention used for the derivations to follow. Again, note that the quantum well is actually assumed to have no thickness despite what is being demonstrated in this figure.

This test was a way to verify if the simulations would agree with a computation done by hand. It is quite extensive to carry out the computations of the matrix multiplications for when the DBR's have a high amount of coupled layers. This case was limited to a single layer making it an equation including 5 matrices. Figure 4.6 is a diagram of the setup. The quantum well is being squeezed between two layers of high index medium with the outer mediums having index of $n_0 = 1.0$ and $n_2 = 3.0$ to reflect the setup of the actual cavity we are testing. The overall transfer matrix, per usual, will then take the following form

$$\begin{pmatrix} E_t \\ 0 \end{pmatrix} = M_I M_P M_{QW} M_P M_I \begin{pmatrix} E_i \\ E_r \end{pmatrix}, \tag{4.9}$$

where M_P is a propagation matrix and M_I is an interface matrix. We limit ourself to the case in which the light is resonant with the medium in the sense that these layers are exactly $\lambda/4$ layers. This simplifies the propagation matrices in particular and gives the following form after evaluating the matrices

$$M_I = \left(\frac{1}{2n_2}\right) \begin{bmatrix} n_2 + n_1 & n_2 - n_1 \\ n_2 - n_1 & n_2 + n_1 \end{bmatrix} \tag{4.10}$$

$$M_p = \begin{bmatrix} e^{\frac{i\pi}{2}} & 0 \\ 0 & e^{-\frac{i\pi}{2}} \end{bmatrix} = \begin{bmatrix} i & 0 \\ 0 & -i \end{bmatrix}. \tag{4.11}$$

applying these to 4.9 then gives this total matrix

$$M_t = \left(\frac{1}{12n}\right) \begin{bmatrix} 3+n & 3-n \\ 3-n & 3+n \end{bmatrix} \begin{bmatrix} i & 0 \\ 0 & -i \end{bmatrix} M_{qw} \begin{bmatrix} i & 0 \\ 0 & -i \end{bmatrix} \begin{bmatrix} n+1 & n-1 \\ n-1 & n+1 \end{bmatrix}, \tag{4.12}$$

where the interface matrices have begun to be evaluated and n is the index of the medium surrounding the quantum well. Performing the matrix multiplication for the outer matrices then give this form

$$M_t = \left(\frac{1}{12n}\right) \begin{bmatrix} i(3+n) & -i(3-n) \\ i(3-n) & -i(3+n) \end{bmatrix} M_{qw} \begin{bmatrix} i(n+1) & i(n-1) \\ -i(n-1) & -i(n+1) \end{bmatrix}. \tag{4.13}$$

The quantity to be tested is the reflectance. Recall that the general solution for incident and reflected field is in terms of the total matrix M

$$M_{21} E_l^+ + M_{22} E_l^- = 0, \tag{4.14}$$

and therefore the reflectance is

$$(M_{21}/M_{22})^2 = R. \tag{4.15}$$

In order to get these exact components from the total matrix, a generalized formula for matrix multiplication was used and then evaluated for the exact components needed.

$$M_{mn} = \sum_{i=1}^{2} a_{mi} \sum_{k=1}^{2} b_{ik} c_{kn}, \tag{4.16}$$

$$M_{21} = a_{21}(b_{11}c_{11} + b_{12}c_{21}) + a_{22}(b_{21}c_{11} + b_{22}c_{21}) \tag{4.17}$$

$$M_{22} = a_{21}(b_{11}c_{12} + b_{12}c_{22}) + a_{22}(b_{21}c_{12} + b_{22}c_{12}). \tag{4.18}$$

The quantum well matrix is evaluated and approximated to be

$$M_{qw} = \begin{bmatrix} 0 & -1.0 \\ 1.0 & 2.0 \end{bmatrix}, \tag{4.19}$$

$$M_{21}/M_{22} = \frac{[a_{21}(b_{11}c_{11} + b_{12}c_{21}) + a_{22}(b_{21}c_{11} + b_{22}c_{21})]}{[a_{21}(b_{11}c_{12} + b_{12}c_{22}) + a_{22}(b_{21}c_{12} + b_{22}c_{12})]}. \tag{4.20}$$

which is approximated to give the following relation

$$\boxed{\frac{M_{21}}{M_{22}} = \frac{[c_{11} - 2c_{21}]}{[c_{12} - 2c_{22}]}} \tag{4.21}$$

Various terms fall off for either being 0 or fractionally small when compared to other quantities (say the 6 from the $3 + n$ term versus the 0.1 from the $3 - n$ term). Evaluating this when $n = 3.0$ gives the following:

$$\frac{[n + 1 - 2 + 2n]}{[1 - n - 2n - 2]} = \frac{[-n + 3]}{[-n - 3]} \approx 0, \tag{4.22}$$

which agrees with the data showing that there is validity to the approximations made and to the simulations. Figure 4.7 shows these behaviors as you approach this resonance. Note that the center agrees with the approximation that at resonance the reflectance is zero

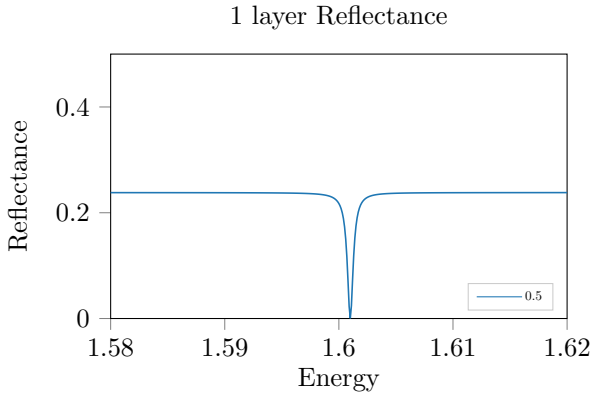

Figure 4.7: Reflectance of single layer cavity as a function of energy corresponding to different frequencies of light.

Note that the outer region of the band is approximately 0.25 which is the natural reflection between a medium with index 1.0 and index 3.1.

$$R = (\frac{3.1 - 1.0}{3.1 + 1.0})^2 \approx 1/4. \tag{4.23}$$

4.4 Exponential Decay of Response Function

The phenomenological approach requisites various parameters of the cavity in order to solve for the full electric field at the quantum well. Among those are the HWHM of the empty cavity γ_c (not to be confused with the γ damping parameter to be found in the optical response of the quantum well). This quantity was found numerically using the Transfer Matrix Method in order to verify a decay that should be seen in our response functions. These types of quantities are typically determined experimentally.

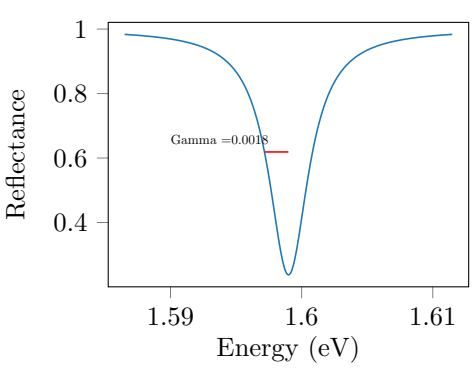

(a) HWHM of Reflectance

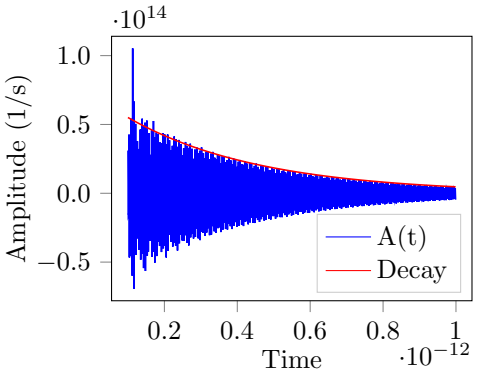

(b) Gamma Decay

Figure 4.8: The HWHM maximum of the empty cavity was deduced numerically as shown in Figure (a). Later it was fitted to Figure (b) to show that the response function of the empty cavity has an exponential decay corresponding to that metric.

Using the same setup as introduced in previous sections in terms of the optical elements and adjusting for the desired resonance, we arrive at the desired metric. As per Figure 4.8a γ was taken to be 0.0018 eV. This was compared and fitted against $\hat{a}(t)$ which is the coefficient in the integrand that emulates the empty cavity. Note that is again using a well defined fourier transform as we are not yet trying to obtain $A(t' - t$ The coefficient should have a decay that corresponds to this metric. Figure 4.8b shows that decay. This test gives another layer of reassurance that our simulations are running as they should but also hinting at how well of an approximation the single-mode cavity equation is.

5 Results

5.1 Preparing the Phenomenological Approach for Comparison

As it stands, the single mode equation is a differential equation that models the field at the quantum well. If given enough information, it can predict various characteristics of the underlying system that is being modeled. In order to compare this model to the transfer matrix approach, it must be solved and manipulated. We manipulate the equations to motivate how a comparison between the two could be made. The electric field at the quantum well can be (in both approaches) deduced to the following relation:

$$E_{QW}(\omega) = a(\omega)E_{inp}(\omega) + b(\omega)P_{QW}(\omega). \tag{5.1}$$

Essentially both approaches can be simplified to a linear relation in frequency space between the full field, the input electric field, and the polarization of the quantum well. Both approaches will differ by the rresults that get you to these coefficients. Previous sections showed how to get these using the transfer matrix approach. As for the phenomenological approach, these coefficients need to be derived from the differential equation:

$$i\hbar\frac{dE_{QW}(t)}{dt} = \hbar\omega_c E_{QW}(t) - \Omega P_{QW}(t) + \hbar t_c E_{inc}^{eff}(t). \tag{5.2}$$

Taking the Fourier transform of both sides leads to the following relation:

$$\hbar\omega\hat{E}_{QW}(\omega) = \hbar\omega_c\hat{E}_{QW}(\omega) - \Omega\hat{P}_{QW}(\omega) + \hbar t_c\hat{E}_{inc}^{eff}(\omega). \tag{5.3}$$

where Ω is proportional to the splitting of the resonant energies between the empty cavity and the LP/UP resonance with the quantum well and t_c is derived from the response properties. The $\hbar\omega_c$ term is defined to be:

$$\hbar\omega_c := \hbar\omega_{cav} - \hbar\omega_0 - i\gamma_c \tag{5.4}$$

where ω_{cav} is the resonant frequency of the cavity, ω_0 is the oscillation frequency of the incoming signal (in this case the fast oscillation frequency of the incoming pulse), and γ_c is related to the HWHM of the reflection curve of the cavity. Rearranging terms we now have:

$$\hat{E}_{QW}(\omega) = \frac{\hbar t_c\hat{E}_{inc}^{eff}(\omega)}{\hbar\omega - \hbar\omega_{cav} + \hbar\omega_0 + i\gamma_c} - \frac{\Omega\hat{P}_{QW}(\omega)}{\hbar\omega - \hbar\omega_{cav} + \hbar\omega_0 + i\gamma_c}. \tag{5.5}$$

Allowing for the two coefficients, $a_{sm}(\omega)$ and $b_{sm}(\omega)$, to be defined as:

$$\begin{aligned} a_{sm}(\omega) &= \frac{\hbar t_c}{\hbar\omega - \hbar\omega_{cav} + \hbar\omega_0 + i\gamma_c} \\ b_{sm}(\omega) &= \frac{\Omega}{\hbar\omega - \hbar\omega_{cav} + \hbar\omega_0 + i\gamma_c} \end{aligned} \tag{5.6}$$

where the subscripts denote that these coefficient are coming form the single mode equations. Another term that needs to be changed is χ. The numerator needs to be replaced with Ω (the rabi splitting as opposed to the 1s exciton wavefunction and the electron dipole moment):

$$\chi(\omega) = -|\vec{d}|^2\frac{|\Omega_{ls}(r=0)|^2}{\hbar\omega - \varepsilon_x + i\gamma_x} \tag{5.7}$$

$$\chi_{sm}(\omega) = -\frac{\Omega}{\hbar\omega - \varepsilon_x + i\gamma_x} \tag{5.8}$$

which allows for a comparison of both approaches. It should be noted that these are evaluated for the case of zero detuning. Here we have allowed for the exciton energy equal to the fast oscillations of our input field $\hbar\omega_{cav} = \hbar\omega_0$. This causes the term in the denominator to be zero for our coefficients.

$$a_{sm}(\omega) = \frac{\hbar t_c}{\hbar\omega - i\gamma_c}$$
$$b_{sm}(\omega) = \frac{\Omega}{\hbar\omega - i\gamma_c} \tag{5.9}$$

In this case, Ω should be equal to half the splitting between the UP and LP energy resonance (as they are equidistant from the empty cavity resonance in this case).

5.1.1 Positive Frequencies and Envelope

The phenomenological approach requires that the input field be in terms of its positive frequencies. In turn, it predicts the electrical field at the quantum well as a function of positive frequencies as well. This breaks certain symmetries found in Fourier transform that force the obtained results to be completely imaginary as opposed to real. Previously, when using symmetric limits of integration, the Fourier transform of the coefficients were completely real. This had to be the case as our field at the quantum well needed to be completely real as well as our input field.

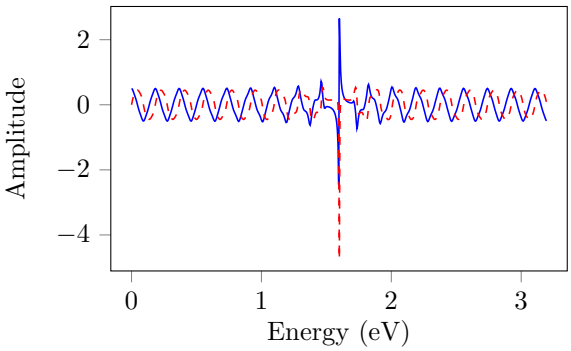

(a) $a(\omega)$ over a larger frequency range. This includes only positive energies and thus was used to determine $A(t)$.

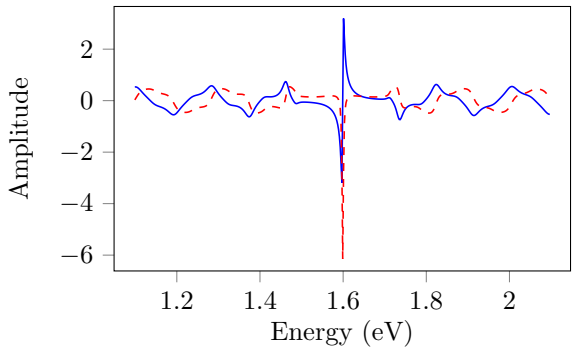

(b) $a(\omega)$ zoomed into the region of resonance. This is to show the symmetries between the real and complex parts.

Figure 5.1: Here we have both the real and imaginary parts of $a(\omega)$ in frequency space. The nature of the integrals can be determined by basic observations of the symmetries shown in these graphs. Of interest is the oscillations found in between resonances. These are a product of using the Transfer Matrix Method over the single-mode equations. These deviations show how the two methods are in disagreement with each other and can be a source of error when choosing the domain of which to integrate over. It is shown later that this error is negligible.

Forcing the limits of integration to no longer be symmetric has the effect of making our coefficients completely imaginary but our input field remains to be real. To obtain the appropriate predictions using only negative frequencies, you simply look at the imaginary part of the electric field of the quantum well. In other words, using only negative frequencies adds an i to the results. This symmetry can be seen in Figure 5.1b. If only positive frequencies are used, the imaginary part of $a(\omega)$ becomes even over the interval and the real part becomes odd.

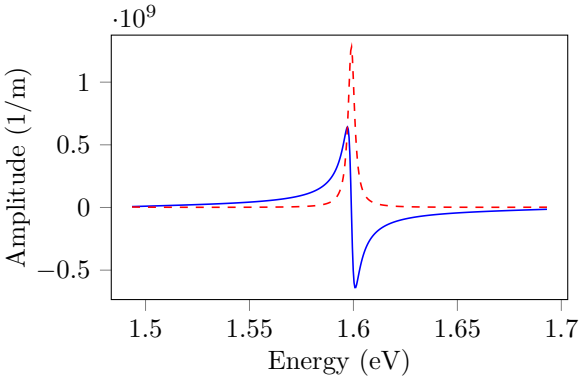

(a) $b(\omega)$ over positive frequencies.

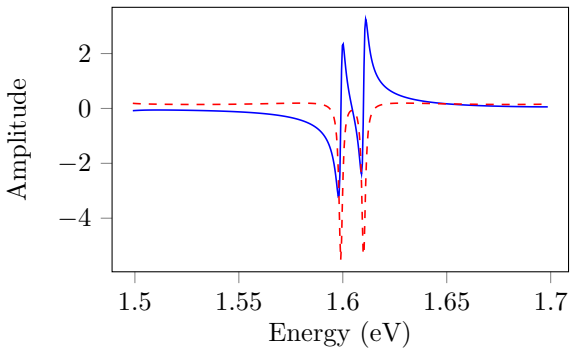

(b) Integrand Coefficient

Figure 5.2: In Figure(a) we have both the real and imaginary parts of $b(\omega)$ in frequency space. Figure (b) shows a combination of $a(\omega)$ and $b(\omega)$ to form all the coefficients used in the integrand.

5.1.2 Cavity Coefficients

The final point of comparison is actually adding the quantum well to both models. This means adding the $b(\omega)$ term and seeing what both models predict. Some algebra is necessary to get the quantum well electric field in terms of the input electric field:

$$\begin{aligned}
E_{QW}(\omega) &= a(\omega)E_{inp}(\omega) + b(\omega)P_{QW}(\omega) \\
E_{QW}(\omega) &= a(\omega)E_{inp}(\omega) + b(\omega)\chi(\omega)E_{QW}(\omega) \\
E_{QW}(\omega) - b(\omega)\chi(\omega)E_{QW}(\omega) &= a(\omega)E_{inp}(\omega) \\
(1 - b(\omega)\chi(\omega))E_{QW}(\omega) &= a(\omega)E_{inp}(\omega) \\
E_{QW}(\omega) &= \frac{a(\omega)}{(1 - b(\omega)\chi(\omega))}E_{inp}(\omega)
\end{aligned} \tag{5.10}$$

where we define a new coefficient

$$C(\omega) = \frac{a(\omega)}{(1 - b(\omega)\chi(\omega))} \tag{5.11}$$

These coefficients completely dictate the response of the cavity. They help relate the incident electric field and polarization to the full field at the quantum well as a linear function. Both models can be reduced to this form and thus give predictions as to what this single coefficient is. What is of interest is the fact that this response function is approximately zero for negative times. This attribute would mean that the response is retarded and thus can be accurately used in the bounded integral.

5.2 Reevaluating the Gaussian Pulse

Taking a second look at the integral in question allows for a different condition to be set in order for the integral to infact be bounded.

$$E_{QW}(t) = \int_{-\infty}^{t} [A(t - t')E^{+}_{inp}(t') + B(t - t')P_{QW}(t')]dt'. \tag{5.12}$$

where $A(t)$ and $B(t)$ are response functions defined by:

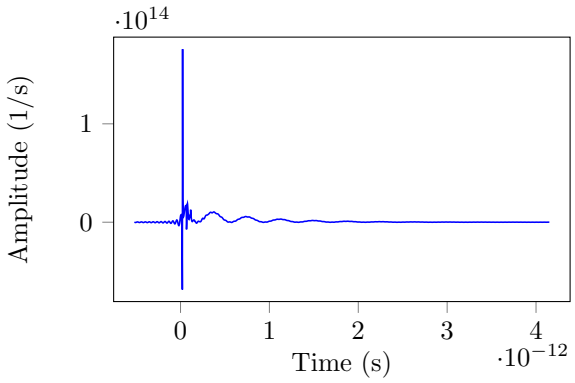

Figure 5.3: This is a plot of $C(t-t')$, the response function used to emulate the entire cavity.

$$A(t-t') = \int_{\omega_{min}}^{\omega_{max}} \frac{d\omega}{2\pi} a(\omega) e^{-i\omega(t-t')}. \tag{5.13}$$

If both the A and B terms are zero for negative times, then the integral can in fact be bounded. ω_{max} and ω_{min} should be defined so as to include the LP and UP resonances and its nearby structures. These can be written in terms of a center frequency ω_0 by defining a $\Delta\omega$:

$$\begin{aligned} \omega_{max} &= \omega_0 + \Delta\omega \\ \omega_{min} &= \omega_0 + \Delta\omega \end{aligned} \tag{5.14}$$

Taking a closer look at these coefficients (or response functions) can serve as evidence as to whether or not this integral can be bounded. They can be combined to form a new coefficient that relates the field at the quantum well to the incident field:

$$\begin{aligned} \begin{pmatrix} E_3^+(\omega) \\ E_3^-(\omega) \end{pmatrix} &= M^L \begin{pmatrix} E_1^+(\omega) \\ E_1^-(\omega) \end{pmatrix} \\ \begin{pmatrix} E_1^+(\omega) \\ E_1^-(\omega) \end{pmatrix} &= \begin{pmatrix} E_{inp}(\omega) \\ -\frac{M_{21}^{total}(\omega)}{M_{22}^{total}(\omega)} E_{inp}(\omega) \end{pmatrix} \\ \begin{pmatrix} E_3^+(\omega) \\ E_3^-(\omega) \end{pmatrix} &= M^L \begin{pmatrix} E_{inp}(\omega) \\ -\frac{M_{21}^{total}(\omega)}{M_{22}^{total}(\omega)} E_{inp}(\omega) \end{pmatrix}. \end{aligned} \tag{5.15}$$

which shows how to express the field in the quantum well region. Recall that the input light is completely forward propagating or $E_{inp} = E_{inp}^+$ The polarization term is then

$$\begin{aligned} P_{QW}(\omega) &= \chi(\omega)(E_3^+ + E_3^-) \\ P_{QW}(\omega) &= \chi(\omega)[(M_{11}^L + M_{12}^L)E_1^+ + (M_{21}^L + M_{22}^L)E_1^-] \\ P_{QW}(\omega) &= \chi(\omega)[(M_{11}^L + M_{12}^L)E_{inp}^+(\omega) + (M_{21}^L + M_{22}^L) - \frac{M_{21}^{total}(\omega)}{M_{22}^{total}(\omega)} E_{inp}^+(\omega)] \\ P_{QW}(\omega) &= \chi(\omega)[(M_{11}^L + M_{12}^L) + (M_{21}^L + M_{22}^L) - \frac{M_{21}^{total}(\omega)}{M_{22}^{total}(\omega)}] E_{inp}^+(\omega). \end{aligned} \tag{5.16}$$

This coefficient is what was used to produce Figure 5.3 in conjuction with 5.13. Evaluating the electric field at the quantum well using a gaussian pulse incident on the cavity shows evidence that the integral can infact be bounded. The question, restated, is simply wether this full integral:

$$E_{QW}(t) = \int_{-\infty}^{\infty} [A(t-t')E^{+}_{inp}(t') + B(t-t')P_{QW}(t')]dt' \tag{5.17}$$

can be accurately approximated with the following bounded integral.

$$E_{QW}(t) \approx \int_{-\infty}^{t} [A(t-t')E^{+}_{inp}(t') + B(t-t')P_{QW}(t')]dt' \tag{5.18}$$

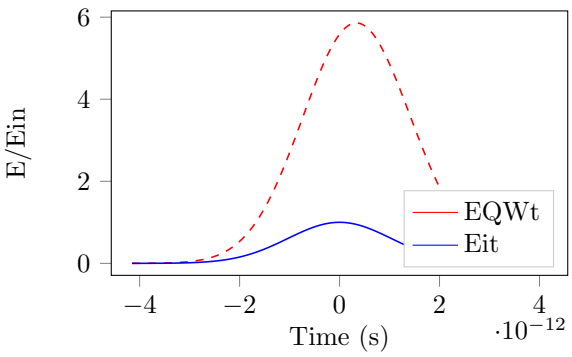

(a) without quantum well

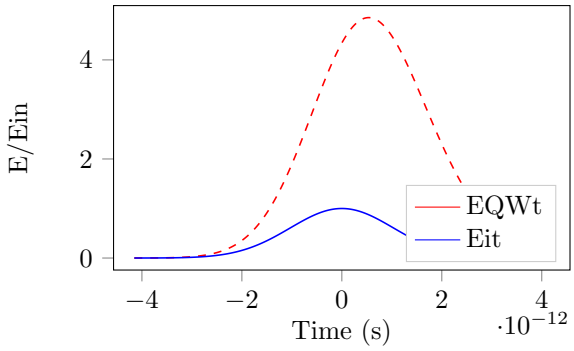

(b) with quantum well

Figure 5.4: This figure shows the results of a gaussian pulse incident on the cavity. Figure (a) shows the response without a quantum well using a gaussian with $\hbar\omega_0 = 1.599eV$ and Figure (b) shows the response with the quantum well using a gaussian with $\hbar\omega_0 = 1.593eV$. These gaussians used the same $\hbar\sigma_\omega$ of $0.9meV$ and therefore each incident pulse had the same pulse duration. A $\hbar\Delta\omega$ of 0.5 eV was used for the domain which corresponds to a $\hbar\omega_{min} = 1.594eV$ and $\hbar\omega_{max} = 1.604eV$ for the second graph and $\hbar\omega_{min} = 1.589eV$ and $\hbar\omega_{max} = 1.598eV$ for the second graph

Of course, the lower bound of the integral also has to be bounded. Since the pulse however is bounded and the evidence from previous sections suggests that the coefficients are zero for negative times, we can set the lower bound such that we begin the integral where the center of the coefficients meets the edge of the pulse. The guassian pulse that was used was of the form.

$$E_{inp}(\omega) = E_0 e^{-(\frac{(\omega-\omega_0)}{\sigma_\omega})^2}. \tag{5.19}$$

Figure 5.4a and 5.4b show the preliminary results of this simulation. It seems as if the integral is infact able to resolve the full field at the quantum well. For this pulse we use a broader pulse so that the gaussian sits better on the LP energy. The simulations were such that the amplitude of the gaussian was unity in frequency domain and the time domain simulations were given in relation to the amplitude of the incident guassian pulse E_{in} in the time domain.

Even though the propose transfer matrix method can be utilized to model the cavity, it isn't without its faults. The model converges to a perfect simulation when you allow the limits of integration to extend to infinity. Depending on the domain used to define the response function, you allow the integrals to see other structures. This makes the model sensitive to that parameter. There is also a discrepency between the bounded time convolution integral and the full fourier integral. This is due to the small but nonzero values that the response function has for negative times.

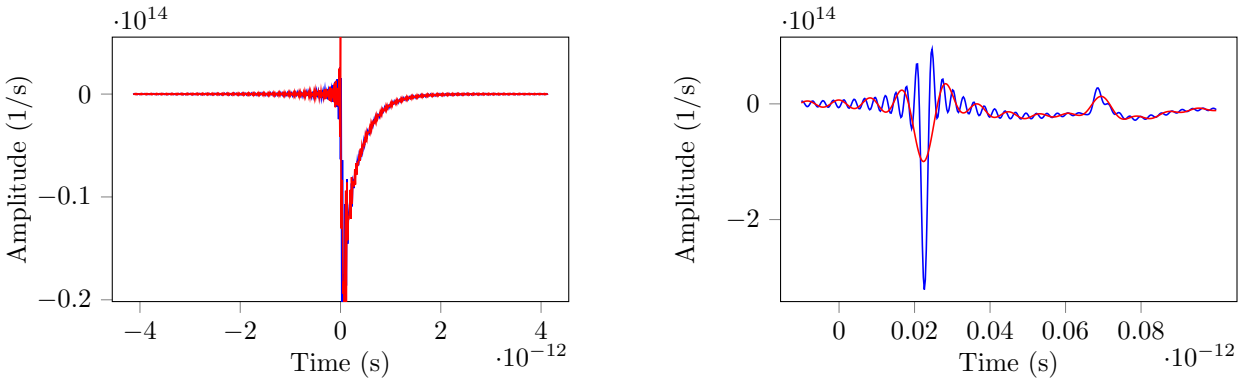

Figure 5.5: $A(t)$ obtained using different domains. The blue curve used an $a(\omega)$ that extended to 1.5 eV outside resonance on both of its sides (corresponding to a domain width of 3 eV) while the red curve extend only to 0.5 eV. The larger domain saw more of the outer oscillating structures of $a(\omega)$ causing the discrepancy. The graph on the right had better resolution which allowed for resolving the oscillations due to using a wider domain.

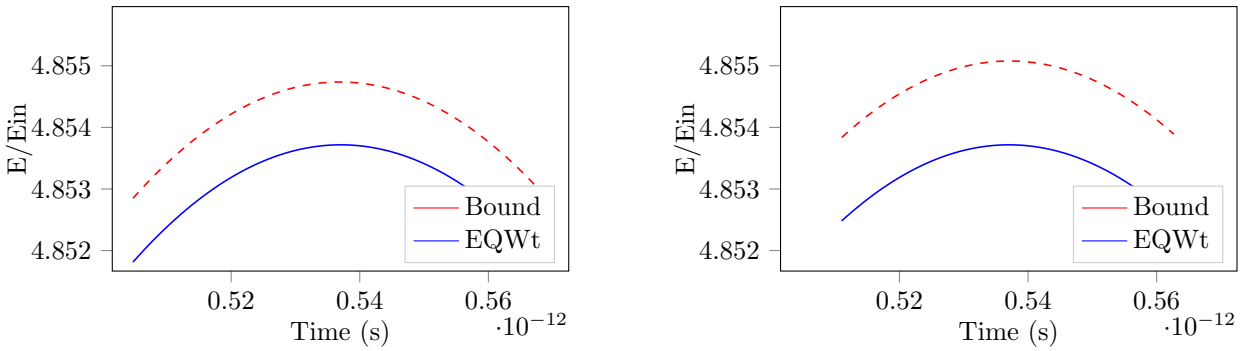

(a) $\hbar\Delta\omega$ of 0.5 eV

(b) $\hbar\Delta\omega$ of 1.5 eV

Figure 5.6: The results demonstrate not only the discrepancies between the integrals but also the senstivity of the model to using a larger domain. It is with this resolution that you can see the negligible difference between the different integrals. The red dashed curve is the bounded integral and the blue is the full integral. Like Figure 5.4b a $\hbar\omega_0 = 1.593eV$ was usd but using different frequency domain widths.

Figure 5.5 is an example of the sensitivity of the response function to the size of the domain used. Each curve was later used as a response function to produce Figure 5.6a and 5.6b. The difference between the integrals is orders of magnitude smaller than the pulses themselves. The quantities in this figure are given in terms of E_{in} which is the amplitude of the gaussian pulse in the time domain. This is all evidence of the response function being retarded and that the convolution integral can infact be bounded.

Appendix

```
import numpy as np

'''
This first set of code serves as the small library of functions I created to carry
out the more compound simulations.

These next 3 functions create the different matrices. It is generalized
so that they can be constructed with a set of input parameters'''

def Propagation(delz,ind,wf):
    c0 = 299792458
    t = ((wf*ind)/(c0))*delz*(1j)
    return np.array([[np.exp(t),0],[0,np.exp(-t)]])

def Interface(n1,n2):
    c = (1/(2*n2))
    return c*np.array([[n2 + n1,n2 - n1],[n2-n1,n2+n1]])

def QWell(wf,n):
    A = 10**(-10)#------------------------------------------ angstrom
    hbar = 6.582119514e-16#--------------------------------- hbar in eV * s
    c0 = 299792458#----------------------------------------- speed of light
    gamma = (137.035999139)**(-1)#-------------------------- fine structure constant
    e = np.sqrt((hbar * (c0))*gamma)#----------------------- charge of electron
    d = -(e) * 10 * A#-------------------------------------- dipole moment
    a0 = 170 * A#------------------------------------------- bhor radius
    X = -((d ** 2) * (8/((a0**2)*np.pi)))/ (abs(hbar * wf) - 1.601  + (1j * 0.0002))  #<-----
        Here is my computation for chi. wf is the frequency
    c = (2 * np.pi * (1j) * (wf / (c0 * n))) * X  #<---- this puts it all together for to
        simplify the returned array. n is the index of the surrounding material (3.1)
    M = np.array([[1,0],[0,1]]) + c*np.array([[1,1],[-1,-1]])
    return M

'''
These next two functions are functions that spit out a list of matrices that
correspond to their names. They also take in parameters corresponding to the
inputs you need to construct them. One function creates a list of matrices
corresponding to the DBR and the other corresponding to the total cavity (which
uses the DBR function).

'''
def DBR(w,layers = 17.5):
    '''
    Function that return a list of matrices corresponding to a DBR
    '''
    lind = [3.6,3.1,3.6]
    enrgy = 1.599
    hbar = 6.582119514e-16
    c0 = 299792458
    prevind = 3.1
    M = []
    for j in range(int(layers*2.0)):
        ind = lind[(-1)**j]
        if j !=0:
            M += [Interface(prevind,ind)]
        L = (np.pi*hbar*c0)/(2*ind*enrgy)
        M += [Propagation(L,ind,w)]
        prevind = ind
    return M

def Cavity(Energy,QW,layers=17.5):
    '''
```

```
    Function that return a list of matrices corresponding to the full cavity

    DBR -> QW -> DBR

    A bool argument is expected to tell the function whether or not to have a quantum
    well in the configuration
    '''
    hbar = 6.582119514e-16
    warr = Energy/hbar

    MEntrance = Interface(1.0,3.0)
    MQWell = QWell(warr,3.1)
    MExit = Interface(3.1,3.0)
    if QW:
        MTotal = [MEntrance] + DBR(warr,layers) + [MQWell] + DBR(warr,layers) + [MExit]
    else:
        MTotal = [MEntrance] + DBR(warr,layers) + DBR(warr,layers) + [MExit]
    return MTotal



def CavityRef(enrgy,QW=False,layers=17.5):
    '''
    This next function just creates the transmittance/reflectance bands of the cavity
    for referencing. It takes in an array of energies and returns the corresponding
    reflectances and transmittance. Optionally you can remove the quantum well from the
    cavity and vary the number of layers
    '''
    ER = []
    ET = []
    for e in enrgy:
        MT = Cavity(e,QW,layers)
        Mi = MT[0]
        for m in MT[1:]:
            Mi = np.matmul(m,Mi)
        E = np.linalg.solve(Mi,np.array([1,0]))
        ER += [np.real(E[1]*np.conj(E[1]))/(E[0]*np.conj(E[0]))]
        ET += [np.real(1/(E[0]*np.conj(E[0])))]
    return ER,ET


def EfieldSimul(energy,qwbool):

    '''
    This function returns the value of the electric field amplitude at each interface
    within the cavity. In a sense it gives you the electric field as a function of
    distance. Again, there is a bool argument that allows you to put in or take out
    the quantum well. The energy is exptected to be a single value corresponding
    to the frequency of light you are interested in.

    '''
    Z = [0]
    EField = []

    hbar = 6.582119514e-16
    c0 = 299792458
    MT = Cavity(energy,qwbool)
    Mi = MT[0]
    for i,m in enumerate(MT):
        if i!=0:
            Mi = np.matmul(m,Mi)
    E = np.linalg.solve(Mi,np.array([1,0]))
    Ei = np.real((E[0]+E[1])*np.conj(E[0]+E[1]))
    #r = Mi[1,1]/(-(Mi[0,1]*Mi[1,0])+(Mi[0,0]*Mi[1,1]))
    #l = Mi[0,1]/((Mi[0,1]*Mi[1,0])-(Mi[0,0]*Mi[1,1]))
```

```
    for i,m in enumerate(MT):
        E = np.matmul(m,E)
        if i%2 == 1:
            et = E[0]+E[1]
            EField += [np.real(et*np.conj(et))/Ei]

    lind = [3.6,3.1,3.6]
    enrgy = 1.599
    for j in range(70):
        ind = lind[(-1)**j]
        l = (np.pi*hbar*c0)/(2*ind*enrgy)
        Z += [Z[-1] + l]
    return Z[1:], EField

def LeftCavitySimul(energy):
    '''
    Function that solves for the electric field amplitude exactly
    at the quantum well. It solves the matrix equation and returns
    the array after it propagates to the QW. It expects a single value
    as its argument which is an energy corresponding to the frequency of light
    you are interested in
    '''
    hbar = 6.582119514e-16
    c0 = 299792458
    MT = Cavity(energy,True)
    Mi = MT[0]
    for i,m in enumerate(MT):
        if i!=0:
            Mi = np.matmul(m,Mi)
        if i==69:
            Mr = Mi
    E = np.array([1,-Mi[1,0]/Mi[1,1]])
    E = np.matmul(Mr,E)
    return E

def scancavity():
    '''
    Function that scans for the LP and UP resonances
    '''
    Energy = np.arange(1.5,1.7,0.0001)
    boo = True
    ER = CavityRef(Energy,boo)[0]
    E1 = Energy[ER.index(min(ER[:int(len(ER)/2.0)]))]
    E2 = Energy[ER.index(min(ER[int(len(ER)/2.0):]))]
    return E1,E2

def timeofflight():
    '''
    Function that returns the time of flight it takes for light to
    propagate to the center of the cavity
    '''
    hbar = 6.582119514e-16
    c0 = 299792458
    enrgy = 1.599
    t = 0
    for j in range(35):
        t += (np.pi*hbar)/(2*enrgy)
    return t

def coeff(e,l):
    '''
    Function that returns the two coefficients that are used in the integrand to have
    the electric field at the quantum well as a function of input light and polarization.
    '''
    MC = Cavity(e,False,layers=l)
```

```
    Ml = MC[0]
    Mr = MC[70]
    for i in range(int(len(MC)/2)):
        if i!=0:
            Ml = np.matmul(MC[i],Ml)
            Mr = np.matmul(MC[i+70],Mr)
    Mt = MC[0]
    for i,m in enumerate(MC):
        if i!=0:
            Mt = np.matmul(m,Mt)
    a = (Ml[0,0] + Ml[1,0]) - (Mt[1,0]/Mt[1,1])*(Ml[1,1] + Ml[0,1])
    b = -(Ml[1,1] + Ml[0,1])*(1/Mt[1,1])*(Mr[1,0] - Mr[1,1])*2*np.pi*(1j)*(w/(c0*3.1))
    return a,b

'''
Code for the cavity without the quantum well. The dz parameter seperates the
DBRs to any length you set it to. The code is shown explicitly as it directly
corresponds to a section in the thesis (which will be the case for the all the code
that is to follow). The reflectance and transmittance were binned for evaluation'''

ER = []
ET = []
for e in Energy:
    warr = e/hbar
    dz = 50*(np.pi*hbar*c0)/(2*3.1*1.599)
    MP = Propagation(dz,warr,3.1)
    MEntrance = Interface(1.0,3.0)
    MExit = Interface(3.1,3.0)

    MT = [MEntrance] + DBR(warr)+[MP]+ DBR(warr) + [MExit]
    Mi = MT[0]
    for m in MT[1:]:
        Mi = np.matmul(m,Mi)
    E = np.linalg.solve(Mi,np.array([1,0]))
    ER += [np.real(E[1]*np.conj(E[1]))/(E[0]*np.conj(E[0]))]
    ET += [np.real(1/(E[0]*np.conj(E[0])))]

'''
This just shows the paramaters used to create the narrow gaussian pulse (narrow in time). It
    was later
processed to resolve the signal at the quantum well. The for loop in the code manipulates
    the input gaussian
and transforms it according to how the cavity behaves. Eiw is the input field in frequency
    domain,
Eit is the field in time domain, EQw the quantum well field in frequency domain, and finally
    EQWt
the quantum well field in time domain.
'''

hbar = 6.582119514e-16
E1,E2 = scancavity()
dE = 0.001
Energy = np.arange(-10.0,10.0 + dE,dE)
f = Energy/(2*np.pi*hbar)
f1 = E1/(2*np.pi*hbar)
df = dE/(2*np.pi*hbar)
wid = 1/(2*np.pi*hbar)
dw = wid/np.sqrt(2)
sigt = 1/(2*np.pi*dw)
Eiw = (1/(np.sqrt(2*np.pi)*dw))*(np.exp(-((f-f1)/wid)**2) + (0j) + np.exp(-((f+f1)/wid)**2))

T = np.fft.fftfreq(len(Energy),d=df)
T.sort()
dt = T[1]-T[0]
Eit = list(np.fft.fftshift(np.fft.fft(Eiw)))
```

```
EQWw = []
Aw = []
for i,e in enumerate(Energy):
    Ep = LeftCavitySimul(e)
    a = Ep[0]+Ep[1]
    Aw += [a]
    EQWw += [a*Eiw[i]]


EQWt = np.fft.fftshift(np.fft.fft(EQWw))

'''
Here we simulate a dielectric slab. An array was setup so as to manipulate the
index of the dielectric and determine reflectance as a function of this index. This
was later graphed and compared to the results found in literature
'''

R = []
dz = np.arange(0.01,3,0.01)
Mode = np.sin(2*1.5*np.pi*dz)**2
for z in dz:
    n2 = N2[j]
    E = np.array([1,0])
    h = (1.0/(4*n2))
    w = (2*np.pi*c)

    E = Interface(1,1.5).dot(E)
    E = Propagation(z,1.5,w).dot(E)
    E = Interface(1.5,1.0).dot(E)

    R += [np.real((E[1]*np.conj(E[1]))/(E[0]*np.conj(E[0])))]

'''
DBRs created by the simulations were tested with this code against the literature. The
    values
of its reflectances as a function of the number of coupled layers were gathered. R1
    represents
the literature results and R2, the simulated ones.
'''

R1 = []
R2 = []
hbar = 6.582119514e-16
L = range(1,20)

for l in L:
    #DBR vs Born Test
    R1 += [((1 - (3.0/1.0)*(3.1/3.6)**(l*2))/(1 + (3.0/1.0)*(3.1/3.6)**(l*2)))**2 ]

    MT = [Interface(1.0,3.1)] + DBR(1.599/hbar,layers=l) + [Interface(3.6,3.0)]
    Mi = MT[0]
    for i,m in enumerate(MT):
        if i!=0:
            Mi = np.matmul(m,Mi)
    E = np.linalg.solve(Mi,np.array([1,0]))
    R2 += [np.real((E[1]/E[0])**2)]


'''
This small bit of code utilized the functions defined earlier to test the single
layer case. The reflectances were binned as a function of energy. This energy of course
is the energy corresponding to the frequency of light being used
'''
```

```
Energy = np.arange(1.58,1.62,0.0001)
L = [0.5]
R = []
for i in L:
    R += [CavityRef(Energy,True,layers=i)[0])]

'''
Here we have the input parameters and the processing techniques used for the
broad gaussian pulse (in time). Like the narrow gaussian, it was processed using
fourier techniques.

'''

hbar = 6.582119514e-16
E1,E2 = scancavity()
dE = 0.0001
Energy = np.arange(-10.0,10.0 + dE,dE)
f = Energy/(2*np.pi*hbar)
f1 = E1/(2*np.pi*hbar)
df = dE/(2*np.pi*hbar)
wid = 0.001/(2*np.pi*hbar)
dw = wid/np.sqrt(2)
sigt = 1/(2*np.pi*dw)
Eiw = (1/(np.sqrt(2*np.pi)*dw))*(np.exp(-((f-f1)/wid)**2) + (0j) + np.exp(-((f+f1)/wid)**2))


T = np.fft.fftfreq(len(Energy),d=df)
T.sort()
dt = T[1]-T[0]
Eit = list(np.fft.fftshift(np.fft.fft(Eiw)))

EQWw = []
Aw = []
for i,e in enumerate(Energy):
    Ep = LeftCavitySimul(e)
    a = Ep[0]+Ep[1]
    Aw += [a]
    EQWw += [a*Eiw[i]]


EQWtfour = np.fft.fftshift(np.fft.fft(EQWw))
At = list(np.real(np.fft.fftshift(np.fft.fft(Aw))))

'''
Here is the code used to make the final results. This include specifically
how the gaussian was modeled and certain response fuctions were obtained.
'''

hbar = 6.582119514e-16
E1,E2 = scancavity()
E0 = 1.599
dE = 0.0001*3
delE = int(abs(E2-E0)/dE)
Energy = np.arange(-1.5,1.5,dE) #<------- Width of domain for A(t-t')
df = dE/(2*np.pi*hbar)
f = Energy/(2*np.pi*hbar)
f1 = E0/(2*np.pi*hbar)
dw = dE/hbar
wid =  0.5*0.0072/(8*np.pi*hbar)
sigt = 1/(2*np.pi*dw)
Eiw = np.exp(-((f)/wid)**2) + (0j) #+ np.exp(-((f+f1)/wid)**2))

w0 = E1/hbar
t0 = 2*np.pi/w0
```

```
dt = t0/10.
T = np.arange(-t0*1600,t0*1600,dt)

Eit = np.zeros(len(T)) + np.zeros(len(T))*(1j)
EQWt = np.zeros(len(T)) + np.zeros(len(T))*(1j)
cit = np.zeros(len(T)) + np.zeros(len(T))*(1j)
for i,e in enumerate(Energy):
    a = coeff(e+E1,17.5)
    c = a[0]/(1-a[1])
    Eit += Eiw[i]*((dw/(2*np.pi)))*np.exp((-1j)*(e/hbar)*T)
    EQWt += Eiw[i]*c*((dw/(2*np.pi)))*np.exp((-1j)*(e/hbar)*T)
    cit += c*((dw/(2*np.pi)))*np.exp((-1j)*(e/hbar)*T)
    if i%100 ==0:
        print(round(i/len(Energy),2))

EQWtconv = np.convolve(dt*cit,Eit,'same')

'''
A different method was used here for obtaining the fourier transforms. Instead
of using the built in function through the numpy package, a discrete fourier
transform was used instead. The summation, although slower, made it much clearer
what was happening to the signals. It allowed for easier manipulation of the time
intervals used.
'''

EQWtbound = []
ab = int(len(T)/2.0)*[0] + list(reversed(cit[-int(len(T)/2.0)-1:]))
for i in range(len(T)):
    if i%100 == 0:
        print(round(i/len(T),2))
    i +=1
    a = ab[-i:]
    b = Eit[:i]
    EQWtbound += [dt*np.dot(a,b)]
```

References

[1] V. Ardizzone, P. Lewandowski, Y.C. Tse, N.H. Kwong, M.H. Luk, A. Lücke, M. Abbarchi, E. Baudin, E. Galopin, J. Bloch, A. Lemaitre, P.T. Leung, P. Roussignol, R. Binder, J. Tignon, and S. Schumacher. Formation and control of Turing patterns in a coherent quantum fluid. *Scientific Reports*, 3:3016, 2013.

[2] Max Born and Emil Wolf. *Principles of Optics*. Pergomon Press, Oxford, 1980.

[3] G. Khitrova, H. M. Gibbs, F. Jahnke, M. Kira, and S. W. Koch. Nonlinear optics of normal-mode coupling semiconductor microcavities. *Reviews of Modern Physics*, 71:1591–1639, 1999.

[4] N. H. Kwong, C. Y. Tsang, M. H. Luk, Y. C. Tse, P. Lewandoswski, C. K. P. Chan, P. T. Leung, S. Schumacher, and R. Binder. *Journal of the Optical Society of America B 33 (7)*, C153, 2016.

[5] N. H. Kwong, C. Y. Tsang, M. H. Luk, Y. C. Tse, P. Lewandoswski, C. K. P. Chan, P. T. Leung, S. Schumacher, and R. Binder. *Physica Scripta 92*, 034006, 2017.

[6] X. Liu, T. Galfsky, and Z. Sun. et al. Strong light–matter coupling in two-dimensional atomic crystals. *Nature Photon*, 9:30–34, 2014.

[7] M. H. Luk. *Pattern Generation and Control in Semiconductor Quantum Well Microcavities*. PhD thesis, 2018.

[8] M.H. Luk, Y.C. Tse, N.H. Kwong, P.T. Leung, P. Lewandowski, R. Binder, and S. Schumacher. Transverse optical instability patterns in semiconductor microcavities: Polariton scattering and low-intensity all-optical switching. *Physical Review B*, 87:205307, 2013.

[9] S. M. H. Luk, P. Lewandowski, N. H. Kwong, C. K. P. Chan, P. T. Leung, S. Schumacher, and R. Binder. *Proceedings of SPIE 10102*, 10102D, 2017.

[10] N. Peyghambarian, S. W. Koch, and A. Mysyrowicz. *Introduction to Semiconductor Optics*. Prentice Hall, New Jersey, 1993.

[11] B.E.A. Saleh and M.C. Teich. *Fundamentals of photonics*. Wiley, New York, 2nd edition, 2006.

[12] J. Sipe. New green-function formalism for surface optics. *J. Opt. Soc. B*, 4:481 – 489, 1987.